NACA RM L50K14

NACA

RESEARCH MEMORANDUM

AN INVESTIGATION OF A SUPERSONIC AIRCRAFT CONFIGURATION HAVING A TAPERED WING WITH CIRCULAR-ARC SECTIONS AND 40° SWEEPBACK

FORCE CHARACTERISTICS OF THE COMPLETE CONFIGURATION AND ITS VARIOUS COMPONENTS AT MACH NUMBERS OF 1.40 AND 1.59

By Norman F. Smith and Jack E. Marte

Langley Aeronautical Laboratory
Langley Field, Va.

NATIONAL ADVISORY COMMITTEE
FOR AERONAUTICS

WASHINGTON

January 22, 1951
Declassified June 24, 1958

NATIONAL ADVISORY COMMITTEE FOR AERONAUTICS

RESEARCH MEMORANDUM

AN INVESTIGATION OF A SUPERSONIC AIRCRAFT CONFIGURATION HAVING A TAPERED WING WITH CIRCULAR-ARC SECTIONS AND 40° SWEEPBACK

FORCE CHARACTERISTICS OF THE COMPLETE CONFIGURATION AND ITS VARIOUS COMPONENTS AT MACH NUMBERS OF 1.40 AND 1.59

By Norman F. Smith and Jack E. Marte

SUMMARY

A force investigation of a supersonic aircraft configuration and various combinations of its components has been conducted in the Langley 4- by 4-foot supersonic tunnel. The tests were performed at Mach numbers of 1.40 and 1.59 at a Reynolds number of approximately 0.6×10^6 based on the wing mean aerodynamic chord and are a part of an extensive investigation of the force and pressure-distribution characteristics of this configuration.

The wing of the model was swept back 40° and had an aspect ratio of 4 with 10-percent-thick circular-arc sections normal to the quarter-chord line. Although for the Mach numbers of the present investigation the wing leading edge was supersonic, a detached shock wave existed at the leading edge throughout the angle-of-attack range.

Longitudinal- and lateral-force characteristics of the various configurations, along with longitudinal- and lateral-stability derivatives, are presented. The data have been analyzed to obtain the aerodynamic characteristics of the components and such interference effects as can be isolated. Comparisons with theory and with the results of the pressure investigations are made.

INTRODUCTION

An investigation has been conducted in the Langley 4- by 4-foot supersonic tunnel to determine the aerodynamic characteristics of a relatively large size model of a swept-wing supersonic aircraft configuration. Tests have been conducted on both a force and pressure model of identical configuration at Mach numbers of 1.40 and 1.59 at a Reynolds number of approximately 0.6×10^6 based on wing mean aerodynamic chord. References 1 to 8 present the results of various phases of this investigation. Tests of a small-scale model of the same configuration in the Langley 9-inch supersonic tunnel are reported in reference 9. An investigation of a rocket-powered model of the same configuration is reported in reference 10.

The present paper deals with the longitudinal- and lateral-force characteristics of the complete aircraft configuration and of various combinations of its components. The data have been analyzed insofar as possible to show the aerodynamic characteristics of each component and the interferences between components. Also included for comparison are some of the integrated pressure results for the wing from reference 3.

The force-model configurations tested were built up by adding to the basic sting-mounted body of revolution in various combinations the canopies, wing, vertical tail, and horizontal tail. The effects of wing-tip skids and stall-control vanes mounted on the wing were also determined.

COEFFICIENTS AND SYMBOLS

The results of the tests are presented in terms of standard NACA coefficients and are referenced to the stability axes shown in figure 1. The reference center of gravity (fig. 2) is at the 25-percent point of the mean aerodynamic chord.

The coefficients and symbols are defined as follows:

C_L lift coefficient $\left(\frac{\text{Lift}}{qS} \text{ where } \text{Lift} = -Z\right)$

C_N normal-force coefficient (Normal force/qS)

C_{L_F} lift coefficient based on frontal area of body of revolution (Lift/qF)

C_D drag coefficient (Drag/qS)

C_C	chord-force coefficient (Chord force/qS)
C_{D_F}	drag coefficient based on frontal area of body of revolution (Drag/qF)
C_m	pitching-moment coefficient ($M'/qS\bar{c}$)
C_{m_F}	pitching-moment coefficient based on frontal area of body of revolution ($M'/qF\bar{c}$)
C_Y	lateral-force coefficient (Y/qS)
C_n	yawing-moment coefficient (N'/qSb)
C_l	rolling-moment coefficient (L'/qSb)
Z	force along Z-axis, pounds
Y	force along Y-axis, pounds
M'	moment about Y-axis, pound-feet
N'	moment about Z-axis, pound-feet
L'	rolling moment about X-axis, pound-feet
q	free-stream dynamic pressure, pounds per square foot
M	Mach number
S	wing area, 1.158 square feet
F	frontal area of body of revolution, 0.0564 square foot
b	wing span, 2.155 feet
c	wing-section chord, feet
$\bar{c}$	wing mean aerodynamic chord, 0.577 foot $\left(\frac{2}{S}\int_0^{b/2} c^2 dy\right)$
y	distance along wing span, from airplane center line
α	angle of attack of fuselage center line, degrees
α_w	angle of attack of wing-chord line, degrees

i_t incidence angle of stabilizer chord line with respect to fuselage center line, degrees

ψ angle of yaw, degrees

C_{Y_ψ} lateral-force parameter, rate of change of lateral-force coefficient with angle of yaw, per degree $(\partial C_Y/\partial\psi)$

C_{n_ψ} directional-stability parameter, rate of change of yawing-moment coefficient with angle of yaw, per degree $(\partial C_n/\partial\psi)$

C_{l_ψ} effective-dihedral parameter, rate of change of rolling-moment coefficient with angle of yaw, per degree $(\partial C_l/\partial\psi)$

L/D ratio of lift to drag (C_L/C_D)

$\partial C_m/\partial\alpha$ rate of change of pitching-moment coefficient with angle of attack

C_{L_α} lift-curve slope at trim $(\partial C_L/\partial\alpha)$

APPARATUS AND TESTS

Tunnel

The Langley 4- by 4-foot supersonic tunnel is a rectangular, closed-throat, single-return wind tunnel designed for a nominal Mach number range of 1.2 to 2.2. The tunnel is described in reference 1. The present series of tests were made at Mach numbers of 1.40 and 1.59 at a stagnation pressure of 0.25 atmosphere.

Model and Support System

A dimensional three-view drawing of the model is shown in figure 2. The geometric characteristics are given in table I; the fuselage and canopy ordinates are given in reference 1. For the investigation reported herein, the wing was equipped with flat-sided ailerons with a blunt trailing edge having a thickness 0.5 of the thickness at the hinge line. Measurements of the model wing showed that the right wing tip was twisted 0.2° with respect to the left wing tip. Both the ailerons and the rudder were set at 0° for all tests reported herein. The angle of incidence of the horizontal stabilizer was remotely controlled by means of an electric motor housed within the model fuselage. An open slot of appreciable size existed in the vertical tail to permit angular motion of the horizontal stabilizer (fig. 2 or see fig. 4 of reference 7).

The model was constructed largely of steel and was frequently inspected and polished in an attempt to maintain an aerodynamically smooth surface. The wing, horizontal tail, vertical tail, and canopies were made detachable (fig. 3) in order to permit determination of the characteristics of various combinations of component parts.

The model was sting-supported from the rear. The support system (fig. 4) provides angle-of-attack changes in the horizontal plane in such a manner that the model remains approximately in the center of the test section. A photograph of the model installation (at a negative angle of attack) is shown as figure 5. An angle of attack of $\pm 11^\circ$ can be obtained with the model on the tunnel center line, with the limiting factor being the contact of the rear of the sting with the tunnel wall. By traversing the model laterally about 10 inches from the vertical center line, the maximum angle of attack may be increased to 16.3°. By employing stings having fixed bends, this angle-of-attack range can be extended still further. Tests over the range of angle of yaw were run by rotating the model 90° (wing horizontal) on the sting. Also, the model and bent stings could be oriented so that tests could be made in the angle-of-attack plane at fixed yaw angles (wing vertical) or in the angle-of-yaw plane at fixed angles of attack (wing horizontal).

Balance

The model was equipped with an internal six-component wire strain-gage balance. The balance was temperature-compensated and interactions between components were in most cases within the accuracy of the scale reading and therefore were neglected. Forces and moments on the balance were transmitted to a Brown self-balancing potentiometer from which individual readings of the six components were visually recorded. A selector switch was provided for each component which made possible selection of one of four scale ranges appropriate to the load conditions involved.

The balance was calibrated in the laboratory and in place in the tunnel and was checked before, after, and during the series of tests. A discussion of the accuracy of the balance and an analysis of the over-all accuracy of the complete balance system is presented in the appendix of reference 7.

TESTS

Conditions and Procedure

The nominal tunnel and model conditions for all tests are listed in the following table:

M	Stagnation pressure (atm)	Stagnation temperature (°F)	Stagnation dewpoint (°F)	Dynamic pressure (lb/sq ft)	Reynolds number	Range of α (deg)	Range of ψ (deg)	Range of i_t (deg)
1.40	0.25	110	-30	229	600,000	-4 to 16	-6 to 10	4 to -10
1.59	.25	110	-35	223	575,000	-4 to 16	-6 to 10	4 to -10

The following configurations were tested at each Mach number:

1. Body of revolution
2. Fuselage (body of revolution plus canopies)
3. Fuselage plus wing
4. Fuselage plus vertical tail
5. Fuselage plus vertical and horizontal tails
6. Fuselage plus wing plus vertical tail
7. Complete model (fuselage plus wing plus vertical and horizontal tails)
8. Complete model plus stall vanes
9. Complete model plus stall vanes plus wing-tip skids
10. Complete model with $\frac{1}{8}$-inch-wide strip of carborundum grains at 10-percent chord on wing and tails and at 10 percent of length from nose of body.
11. Complete model with slot in the vertical tail filled

Corrections and Accuracy

Calibration data for the M = 1.40 nozzle is presented in reference 2 and for the M = 1.59 nozzle in reference 1. The magnitude of the Mach number variation, flow angle, and pressure gradients in the vicinity of the model are shown to be small, and no corrections have been applied to the data. The maximum variation in Mach number at either Mach number through the region occupied by the model is about ±0.01. The flow angularity in the horizontal plane is within about ±0.2° and in the vertical

plane about 0.30° to -0.11°. Tests made at angles of attack in both planes (reference 6) were in good agreement except for a slight roll asymmetry.

Sting deflection under load was negligible and no angle-of-attack correction was necessary. The angle of attack is accurate to ±0.05°, while the tail incidence is accurate to ±0.1°. Optical measurements made during the tests showed that wing twist under load was small and amounted to less than 0.05° for all angles of attack.

The interference forces caused by the sting support have not been measured and no corrections for these forces have been applied to the data. It is indicated in reference 11 for a similar sting-body combination that the interference forces due to the sting are small; however, the exact magnitude is not known.

As mentioned in a previous section, stings having initial bends of 0°, 3°, and 6° were used to obtain high angles of attack and to obtain combinations of angle of attack and yaw. The effect of the different stings on lift, drag, and pitching moment was found to be insignificant.

Pressure measurements were made at the base of the fuselage for the complete model at $M = 1.59$. These data indicate that the base pressure can be considered to be stream static within the accuracy of the test results, except for the angle-of-attack range from 4° to 10° where a correction decreasing the measured drag by approximately 1 percent would be necessary.

The maximum probable uncertainities in the aerodynamic coefficients (due to the balance system) are as follows:

Pitching moment	±0.00045
Lift	±0.0010
Drag	±0.00025
Lateral force	±0.0010
Rolling moment	±0.0006
Yawing moment	±0.00011

RESULTS AND DISCUSSION

The results of the investigation are presented in two sections. In the first are presented the basic data, which include the aerodynamic characteristics in pitch and yaw of the various configurations as tested. In the second section is presented the analysis of these data, including stability derivatives, characteristics of component parts which can be determined, and such significant interference effects between various components as can be isolated.

Since tests were not made on isolated components (except for the body of revolution) most of the characteristics of component parts include some interference effects. Further, the interference effects which can be determined from the data are usually the net result of mutual interference of several components. Hence, only the interference effects which are of major interest and which can be isolated to a reasonable degree have been presented. Others may be obtained through use of the basic data.

Pressure distributions over wing and fuselage of a configuration identical with the present configuration have been published in references 1 to 3. No pressure data except for forces on the wing obtained by integration of pressure data are shown in the present paper. The analyses of these references are utilized wherever necessary, however, to aid in defining the phenomena indicated by the force results. Also, the discussion of the force characteristics of the various configurations includes some repetition of the results of the detailed investigations of longitudinal and lateral stability reported in references 4, 5, and 6.

For the test Mach numbers of 1.40 and 1.59 the ratios of the cotangent of the sweep angle to the tangent of the Mach angle are 1.06 and 1.34, respectively. Although the component of the free-stream Mach number normal to the wing leading edge is thus supersonic in the usual sense, the combination of sweep angle, Mach number, and leading-edge angle of the wing section results in a detached shock at the wing leading edge for all angles of attack at both Mach numbers. This detached shock leads to a small region of the subsonic flow at the wing leading edge which violates a fundamental assumption of the linear theory. These effects will be evident from the data and from comparisons between experimental and theoretical results. For the Reynolds number of these tests, the boundary layer over the wing and over the fuselage (alone) is basically laminar, according to unpublished results of tests of a body of revolution and the results of reference 3.

Basic Data

Longitudinal.- The variation of lift coefficient (based on wing area) with angle of attack for the various configurations for Mach numbers of 1.40 and 1.59 is shown in figure 6. The curves are nearly linear except at high angles of attack. For configurations which include the wing, the lift-curve slope decreases at the higher angles of attack. This decrease in C_{L_α} is a consequence of laminar separation over the trailing edge and outboard sections of the wing. This loss of lift is to be expected for swept wings and is discussed in detail for this particular wing in reference 3. The value of C_{L_α} at $M = 1.40$ is greater than at $M = 1.59$ as is predicted by theory.

A slight increase in lift-curve slope with increasing angle of attack is noted for configurations which do not include the wing. This increase is a result of flow separation on the fuselage which in this case tends to increase the lift. This phenomenon is discussed in reference 12 where it is shown that due to separation of cross-flow components at angle of attack, the lift on a body of revolution is greater than that calculated by potential theory, in both subsonic and supersonic flow.

The drag characteristics of the various configurations are presented in figure 7. The largest increment in drag results from addition of the wing. A minimum drag coefficient for the complete model of about 0.055 was measured near the zero angle of attack for the wing ($\alpha \approx -3^\circ$). The drag coefficient for the complete configuration is slightly less at $M = 1.59$ than at $M = 1.40$.

The variation of pitching-moment coefficient with angle of attack (fig. 8) for each configuration is essentially linear. The body of revolution and fuselage configurations by themselves are unstable, but the addition of either the horizontal tail or the wing produces a highly stable combination. The static margin for the complete configuration is about 35 percent of the mean aerodynamic chord.

This high degree of stability is due in part to the rearward position of the wing center of pressure. Pressure measurements indicated that the wing-alone configuration would be quite stable at supersonic speeds, although tests at low-subsonic speeds (reference 13) have shown it to be unstable in this low speed range. Also contributing to the high degree of stability of the complete model is the rearward position of the lift carry-over on the fuselage. This rearward position of the lift carry-over has been shown theoretically by Ferrari (reference 14) and others and has been shown by as yet unpublished results of the pressure-distribution tests of this configuration. Reference to figure 6 shows that the maximum trim lift coefficient for the complete model which can be reached with the available stabilizer deflection ($i_t = -10^\circ$) is approximately 0.38 at $M = 1.40$.

Figure 9 presents the longitudinal forces for the complete model up to an angle of attack of 22°. The lift coefficient increased continuously through this range and reached a value of about 0.96 at $\alpha = 22^\circ$, which angle corresponds to a wing angle of attack of 25°. The slope of the lift curve at $\alpha = 22^\circ$ was slightly more than half that at $\alpha = 0^\circ$.

The curves of normal-force coefficient and chord-force coefficient for the complete model are also shown in figure 9 for illustrative purposes, since normal and chord forces are the forces directly measured by the internal strain-gage balance. It is interesting to note that the chord force remains nearly constant as the angle of attack is increased. The large increase in drag which occurs is due entirely to the streamwise component of the normal force.

Lateral.- The variation of lateral-force coefficient with yaw angle is shown in figure 10. As would be expected, the largest increment of side force is that due to the vertical tail. The lateral force measured for the fuselage at moderate and high angles of yaw is twice that measured for the streamline body, although the canopies increase the lateral area of the streamline body by only 24 percent.

The yawing-moment characteristics (fig. 11) show that the configurations without the vertical tail are directionally unstable. The canopies increase the degree of instability of the body of revolution because of the lateral area presented by the canopies on the forward portion of the body. Addition of the wing moves the curve in a stable direction. A smaller stabilizing increment is measured at $M = 1.59$ than at $M = 1.40$, although the lateral-force increments at these Mach numbers are approximately equal. Reference 15 shows that the directional stability of the wing alone may be decreasing with Mach number in this range and may even change sign.

The vertical tail introduces a high degree of directional stability. The horizontal tail, by increasing the effective aspect ratio of the vertical tail, still further increases the directional stability to the relatively high value shown for the complete model. The directional stability is shown to decrease as the Mach number is increased (see section entitled "Stability derivatives").

Figure 12 presents rolling-moment characteristics for an angle-of-yaw range from -6° to 10°. The wing-fuselage combination exhibits negative effective dihedral, due to the low wing position and to the fact that the wing alone probably has very low or possibly negative effective dihedral at these Mach numbers (see reference 16). The positive effective dihedral measured for the complete airplane is due to the contribution of the vertical tail. The small rolling moment shown at $\psi = 0^\circ$ for the configurations which include the wing is due to a slight amount of wing or flow asymmetry.

The drag characteristics of the various configurations in yaw are shown in figure 13. The drag rise in yaw is small and comes mainly from the addition of the vertical tail. There appears to be little change with Mach number.

The effects of angle of attack upon the lateral characteristics of three configurations are shown in figure 14 for $M = 1.59$. In general, increasing the angle of attack reduced slightly the slopes of all curves. The slight variation in the slope of the rolling-moment curve with angle of attack is in contrast with the increase usually obtained at low speeds for similar configurations and is apparently due to compensating effects which cannot be completely isolated. A detailed discussion of this point is presented in reference 6.

Analysis

Stability derivatives.- Numerical values of the basic static-lateral-stability derivatives are given for the complete-airplane configuration at trim conditions in the following table:

Derivative	M = 1.40	M = 1.59
C_{l_ψ}	0.00075	0.00090
C_{n_ψ}	-.00255	-.00184
C_{Y_ψ}	.0147	.0132

The derivatives C_{n_ψ} and C_{Y_ψ} decrease by an appreciable amount when the Mach number is increased from 1.40 to 1.59. This decrease is a consequence of the decrease in lift-curve slope which occurs for these particular airfoil surfaces when the Mach number is increased in this range. The decrease in C_{n_ψ} with Mach number which occurs for this configuration has been observed in other investigations (references 6 and 9) which indicate that at a relatively high Mach number the configuration may become directionally unstable. A comparison of the data of the present paper with other supersonic data is shown in figure 13 of reference 10.

Although the contribution of the vertical tail to the effective dihedral similarly decreases, a small net increase in the value of C_{l_ψ} occurs as a consequence of the change of the effective dihedral of the wing in a positive direction (fig. 10) as the Mach number is increased.

The variations of C_{L_α} and C_{m_α} (at trim) with angle of attack are presented in figure 15 for two Mach numbers. The maximum available stabilizer angle (-10°) was inadequate to produce trim above $\alpha \approx 6^\circ$. The decrease in lift-curve slope (C_{L_α}) which occurs as the Mach number is increased is expected from theoretical considerations for the particular wing involved (reference 3). The decrease in slope of the pitching-moment curve is a result of the decrease in lift-curve slope of the tail. It should be noted that while a decrease in both C_{L_α} and C_{m_α} is encountered at the higher Mach number, only a small change in C_m/C_L occurs (reference 5).

Lift-drag ratios.- The variations of lift-drag ratios with angle of attack for five configurations are shown in figure 16. The complete model was trimmed longitudinally only for angles of attack of -2° to 6°.

The lower L/D exhibited by the complete model, compared with the configuration without horizontal tail, is a consequence of the down load on the horizontal tail required for trim. The highest value of L/D obtained for the complete configuration was approximately 3.3 at $\alpha = 6^\circ$ and $M = 1.40$ and slightly lower at $M = 1.59$. This low value of L/D is due to the fact that the wing has a relatively high thickness ratio (8 percent in the streamwise direction) and inadequate sweep for the Mach numbers involved.

Model breakdown.- The lift, drag, and pitching-moment characteristics of the fuselage with and without canopies are shown in figure 17. Coefficients are based upon the frontal area of the body of revolution. The characteristics of the body of revolution calculated by the linear theory and by the method of reference 12 are also shown in each plot. The linear theory considerably underestimates the lift and pitching moments, while the theory of reference 12, which considers the cross-flow components, indicates good agreement with the experimental results.

Addition of the canopies to the body of revolution results in an increase in drag of 30 to 50 percent at low angles of attack, although the canopies increase the frontal area by only 11 percent. The increment in drag decreases somewhat at high angles of attack. The lift-curve slope for both configurations is low, with the body of revolution exhibiting higher lifts and a higher slope. No significant differences between the moment curves for the two configurations are noted.

The increments in lift and drag coefficients produced by the canopies are larger at $M = 1.40$ than at $M = 1.59$. Approximate calculations show that the shock from the canopy leading edge may be detached at $M = 1.40$ and attached at $M = 1.59$.

Lift-drag ratios for the body of revolution are compared in figure 18 with those for the fuselage in normal orientation and rotated 90° (about its own axis), the latter data being taken from yaw tests of the fuselage. The body of revolution has a higher L/D than the normal fuselage, while the L/D for the fuselage rotated through 90° is higher than that for the normal fuselage at low angles of attack and higher than that for both other configurations at high angles of attack. Basic data show that the rotated fuselage has assumed considerably more lift than the other configurations. Although the rotated fuselage is thus shown to be the most efficient lifting body of the three tested at high angles of attack, in the practical case account must be taken of the fact that it may be desirable to carry as much lift as possible on the wings and as little as possible on the less-efficient fuselage.

The wing characteristics obtained by subtracting the force characteristics of the fuselage alone from those measured from the wing-fuselage combination are compared in figure 19 with the wing characteristics

obtained from the pressure data of reference 3 and with wing characteristics calculated by means of the linear theory. The force characteristics thus obtained of course include mutual interference of fuselage and wing. The experimental pressure data, on the other hand, have been reduced (reference 3) in an effort to obtain wing-alone characteristics by extrapolating spanwise data to the fuselage center line. Of necessity the interference of the fuselage on the wing is, in part, included. The theoretical characteristics were calculated for an isolated wing and do not include effects of shock detachment, separation, skin friction, or interference.

The lift and drag obtained by either force or pressure measurements are lower than predicted by linear theory. This difference is primarily a result of laminar separation at the trailing-edge and at outboard stations (see reference 3). The drag measured in the force tests is slightly higher than that obtained from the pressure-distribution tests. This difference is greater than that which would be expected for skin friction alone, since the laminar and turbulent skin-friction drag coefficients for the wing are 0.002 and 0.005, respectively. The difference is evidently due in part to unfavorable wing-fuselage interference, probably in the form of juncture separation.

The measured effect of Mach number on the lift and drag curves is less than the linear theory predicts. This effect is due to the fact that the theory overpredicts the variations which occur (with Mach number) in the Mach number range where the Mach line is in the vicinity of the leading edge of the wing.

Laminar separation at the trailing edge and a region of subsonic flow at the leading edge are shown in reference 3 to result in a lower degree of stability from the pressure tests than is indicated by theory (fig. 19). In the case of the force data, these same destabilizing effects are compensated by the stabilizing effect of the rearward carry-over of the wing lift on the fuselage. The apparent agreement between the pitching moments obtained from force data and those obtained by means of the theory is therefore coincidental.

Interference.- The effect of the wing on the effectiveness of the horizontal stabilizer is shown in figure 20. The slope of the curves (dC_m/di_t) is slightly lower for the stabilizer operating in the presence of the wing. This effect is believed due to a change in flow conditions at the tail. These changes are most probably due to such factors as shock and wing-fuselage-juncture boundary layer, since for the angle-of-attack range of these tests, the horizontal tail is appreciably above the wing wake.

The effects of the wing and horizontal stabilizer upon the increments of side force, rolling moment, and yawing moment produced by the vertical

tail are shown in figures 21 and 22, respectively. The effect of the wing is small, the largest effect being to increase slightly the slope of the yawing-moment curve.

The horizontal tail (fig. 22) has a small favorable influence upon the vertical tail, due probably to the end-plate effect which increases the effective aspect ratio of the vertical tail. Little change is found in these effects between the two test Mach numbers.

Boundary-layer transition effects.- In an attempt to determine the effects of fixing boundary-layer transition, a $\frac{1}{8}$-inch-wide strip of no. 60 carborundum grains was located at 10 percent of the chord from the leading edge of the wing and tails and at the 10-percent-length station on the fuselage. The results of tests of the complete model at $M = 1.59$ with fixed and natural transition are shown in figure 23. The only significant result of fixing transition is an increase in drag coefficient of the order of 0.006. This value is approximately the same magnitude as the increase in skin-friction drag to be expected if transition from laminar to turbulent flow occurred at the carborundum strip. From the results of reference 17, however, it appears that an increment of the same magnitude or larger should result from the wave drag of the transition strip itself.

The measured drag increment, therefore, appears to be too small to indicate with certainty that transition was actually fixed on the model by the carborundum strip. The low Reynolds number of the flow along with the favorable pressure gradient in the vicinity of the strip may have precluded transition.

Miscellaneous.- The slot in the vertical tail (required by the controllable horizontal stabilizer and illustrated in figure 4 of reference 7) is shown in figure 24 to have a small effect upon the aerodynamic characteristics of the complete model. A slight increase in the lateral force and yawing moment is measured when the slot is filled. No effect upon the lift and drag is shown, although a slight increase in drag too small to be seen in figure 24 was actually measured. The absolute values of pitching-moment coefficient were slightly more positive, which indicates that an effect of sealing the opening might be to shift the tail center of pressure forward.

Figure 25 shows the effect upon the longitudinal and lateral characteristics of the addition of stall-control vanes and wing-tip skids (fig. 2(b)) to the complete model. The effects upon all components are seen to be small or negligible, the largest effects being a slight shift in angle of attack for trim and in the slope of the rolling-moment curve.

CONCLUDING REMARKS

A force investigation of a supersonic aircraft configuration and various combinations of its components has been conducted in the Langley 4- by 4-foot supersonic tunnel at Mach numbers of 1.40 and 1.59 and a Reynolds number of 0.6×10^6. The model employed a tapered 40° swept-back wing with 10-percent-thick circular-arc sections normal to the quarter chord.

The lift and pitching-moment variations for the complete model were essentially linear in the low angle-of-attack range. At the higher angles of attack, however, there was a progressive decrease in lift-curve slope which at angle of attack of 22° was approximately one-half that of 0°. A lift coefficient of 0.96 was attained at a wing angle of attack of 25°. The measured chord force for the complete model remained essentially constant; the drag rise with angle of attack thus resulted entirely from the component of the normal force in the drag direction.

The effects of Mach number within the limited test Mach number range were small but in accordance with linear theory. For the body of revolution (fuselage without canopies) the slopes of the lift and moment curves were greater than those predicted by nonviscous theory but were in accordance with a flow analysis based on fuselage cross-flow components. Addition of the canopies increased both the drag and side force over that of the body of revolution by an amount considerably greater than the proportionate increase in frontal or lateral area.

For the particular center-of-gravity location used (chosen from consideration of low-speed stability) the wing alone was longitudinally stable, while the fuselage alone was unstable. Addition of the wing to the fuselage resulted in a configuration of high longitudinal stability which was produced in part by a stabilizing interference effect of the wing upon the fuselage.

Langley Aeronautical Laboratory
National Advisory Committee for Aeronautics
Langley Field, Va.

REFERENCES

1. Cooper, Morton, Smith, Norman F., and Kainer, Julian H.: A Pressure-Distribution Investigation of a Supersonic Aircraft Fuselage and Calibration of the Mach Number 1.59 Nozzle of the Langley 4- by 4-Foot Supersonic Tunnel. NACA RM L9E27a, 1949.

2. Hasel, Lowell E., and Sinclair, Archibald R.: A Pressure-Distribution Investigation of a Supersonic-Aircraft Fuselage and Calibration of the Mach Number 1.40 Nozzle of the Langley 4- by 4-Foot Supersonic Tunnel. NACA RM L50B14a, 1950.

3. Cooper, Morton, and Spearman, M. Leroy: An Investigation of a Supersonic Aircraft Configuration Having a Tapered Wing with Circular-Arc Sections and 40° Sweepback. A Pressure-Distribution Study of the Aerodynamic Characteristics of the Wing at Mach Number 1.59. NACA RM L50C24, 1950.

4. Spearman, M. Leroy: An Investigation of a Supersonic Aircraft Configuration Having a Tapered Wing with Circular-Arc Sections and 40° Sweepback. Static Longitudinal Stability and Control Characteristics at a Mach Number of 1.40. NACA RM L9L08, 1950.

5. Spearman, M. Leroy, and Hilton, John H., Jr.: An Investigation of a Supersonic Aircraft Configuration Having a Tapered Wing with Circular-Arc Sections and 40° Sweepback. Static Longitudinal Stability and Control Characteristics at a Mach Number of 1.59. NACA RM L50E12, 1950.

6. Spearman, M. Leroy: An Investigation of a Supersonic Aircraft Configuration Having a Tapered Wing with Circular-Arc Sections and 40° Sweepback. Static Lateral Stability Characteristics at Mach Numbers of 1.40 and 1.59. NACA RM L50C17, 1950.

7. Robinson, Ross B.: An Investigation of a Supersonic Aircraft Configuration Having a Tapered Wing with Circular-Arc Sections and 40° Sweepback. Static Lateral Control Characteristics at Mach Numbers of 1.40 and 1.59. NACA RM L50I11, 1950.

8. Spearman, M. Leroy, and Webster, Robert A.: An Investigation at Mach Numbers of 1.40 and 1.59 of the Effects of Aileron Profile on the Aerodynamic Characteristics of a Supersonic Aircraft Configuration. NACA RM L50J31, 1950.

9. Ellis, Macon C., Jr., Hasel, Lowell E., and Grigsby, Carl E.: Supersonic-Tunnel Tests of Two Supersonic Airplane Model Configurations. NACA RM L7J15, 1947.

10. D'Aiutolo, Charles T., and Mason, Homer P.: Preliminary Results of the Flight Investigation between Mach Numbers of 0.80 and 1.36 of a Rocket-Powered Model of a Supersonic Airplane Configuration Having a Tapered Wing with Circular-Arc Sections and 40° Sweepback. NACA RM L50H29a, 1950.

11. Osborne, Robert S.: High-Speed Wind-Tunnel Investigation of the Longitudinal Stability and Control Characteristics of $\frac{1}{16}$-Scale Model of the D-558-2 Research Airplane at High Subsonic Mach Numbers and at a Mach Number of 1.2. NACA RM L9C04, 1949.

12. Allen, H. Julian: Estimation of the Forces and Moments Acting on Inclined Bodies of Revolution of High Fineness Ratio. NACA RM A9I26, 1949.

13. Weil, Joseph, Comisarow, Paul, and Goodson, Kenneth W.: Longitudinal Stability and Control Characteristics of an Airplane Model Having a 42.8° Sweptback Circular-Arc Wing with Aspect Ratio 4.00, Taper Ratio 0.50, and Sweptback Tail Surfaces. NACA RM L7G28, 1947.

14. Ferrari, Carlo: Interference between Wing and Body at Supersonic Speeds - Theory and Numerical Application. Jour. Aero. Sci., vol. 15, no. 6, June 1948, pp. 317-336.

15. Jones, Arthur L., and Alksne, Alberta: The Yawing Moment Due to Sideslip of Triangular, Trapezoidal, and Related Plan Forms in Supersonic Flow. NACA TN 1850, 1949.

16. Jones, Arthur L., Spreiter, John R., and Alksne, Alberta: The Rolling Moment Due to Sideslip of Triangular, Trapezoidal, and Related Plan Forms in Supersonic Flow. NACA TN 1700, 1948.

17. Perkins, Edward W.: Experimental Investigation of the Effects of Support Interference on the Drag of Bodies of Revolution at a Mach Number of 1.5. NACA RM A8B05, 1948.

TABLE I.- GEOMETRIC CHARACTERISTICS OF MODEL

Wing:	
Area, sq ft	1.158
Span, ft	2.155
Aspect ratio	4
Sweepback of quarter-chord line, deg	40
Taper ratio	0.5
Mean aerodynamic chord, ft	0.557
Airfoil section normal to quarter-chord line	10-percent-thick, circular-arc
Twist, deg	0
Dihedral, deg	3
Horizontal tail:	
Area, sq ft	0.196
Span, ft	0.855
Aspect ratio	3.72
Sweepback of quarter-chord line, deg	40
Taper ratio	0.5
Airfoil section	NACA 65-008
Vertical tail:	
Area (exposed), sq ft	0.172
Aspect ratio (based on exposed area and span)	1.17
Sweepback of leading edge, deg	40.6
Taper ratio	0.337
Airfoil section, root	NACA 27-010
Airfoil section, tip	NACA 27-008
Fuselage:	
Fineness ratio (neglecting canopies)	9.4
Frontal area (body of revolution), sq ft	0.0564
Miscellaneous:	
Tail length from $\bar{c}/4$ wing to $\bar{c}_t/4$ tail, ft	0.917
Tail height, wing semispans above fuselage center line	0.153

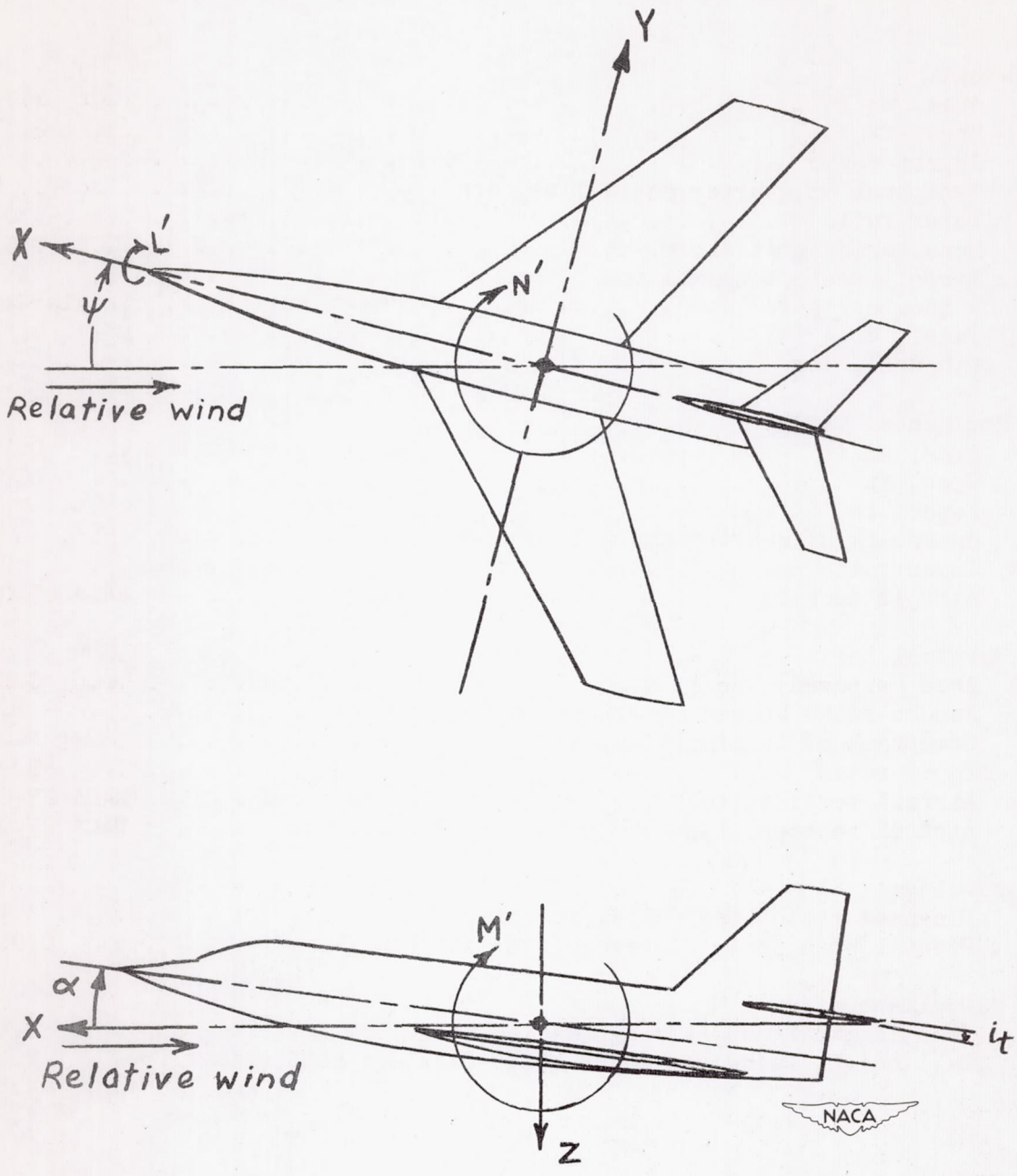

Figure 1.- System of stability axes. Arrows indicate positive values.

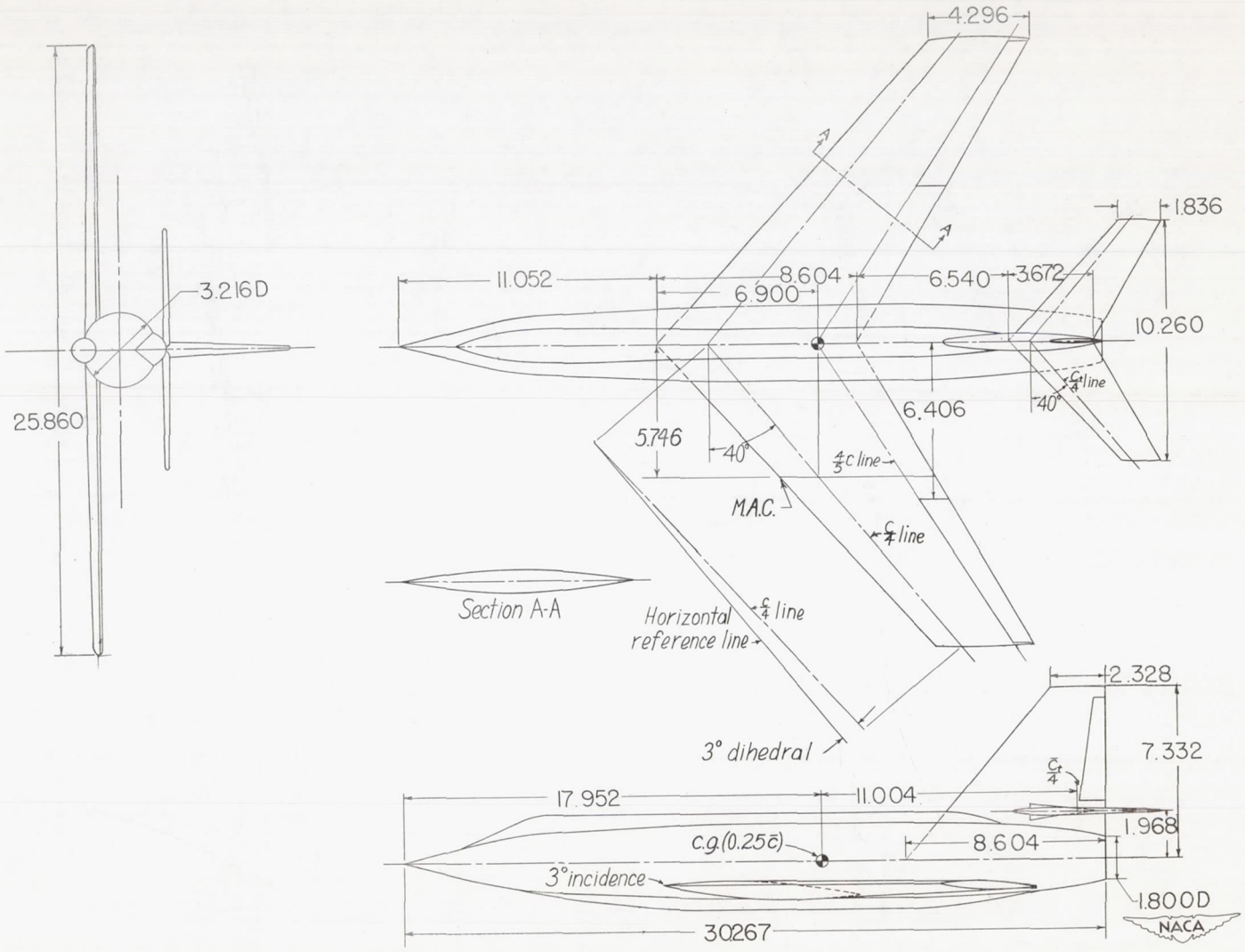

Figure 2.- Details of model of supersonic aircraft configuration.
Dimensions are in inches unless otherwise noted.

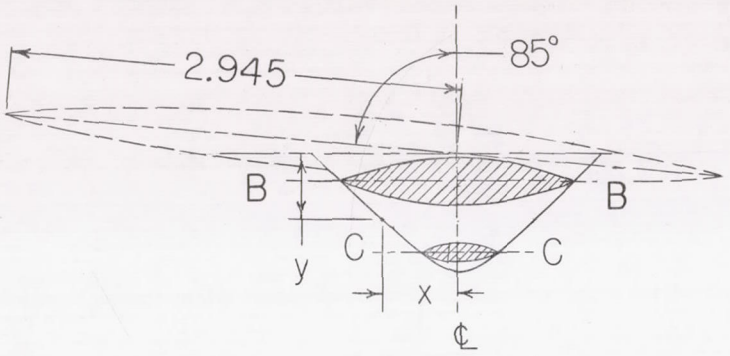

Section A-A

x	y
.879	.000
.677	.202
.459	.420
.241	.639
.000	.740

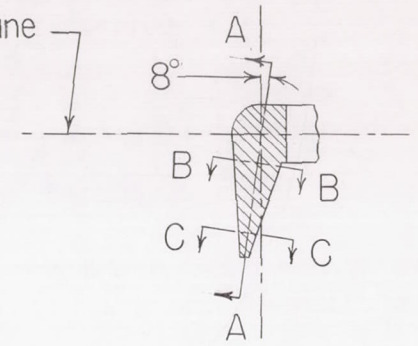

Wing-tip skid

All dimensions in inches

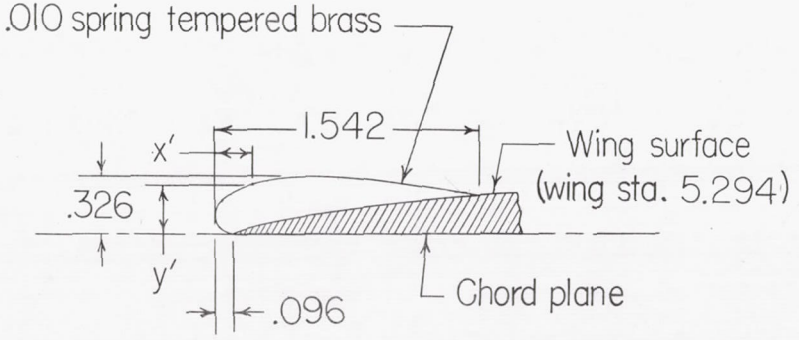

Wing stall-control vane

x'	y'
.096	.000
.000	.090
.133	.233
.267	.281
.533	.319
.733	.326
1.000	.317
1.267	.290
1.533	.183

NACA

Figure 2.- Concluded.

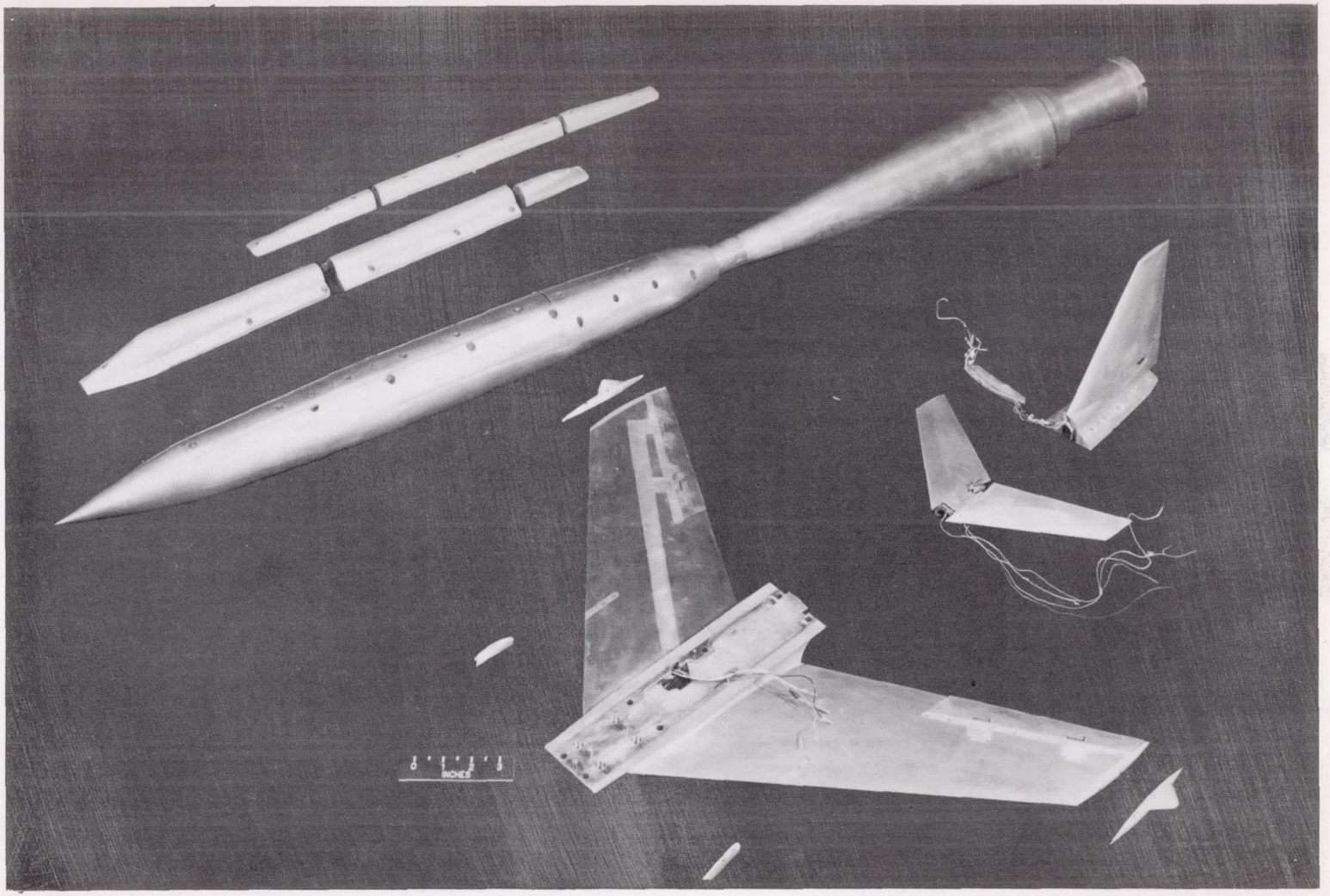

Figure 3.- Component parts of model of supersonic aircraft. L-62218.1

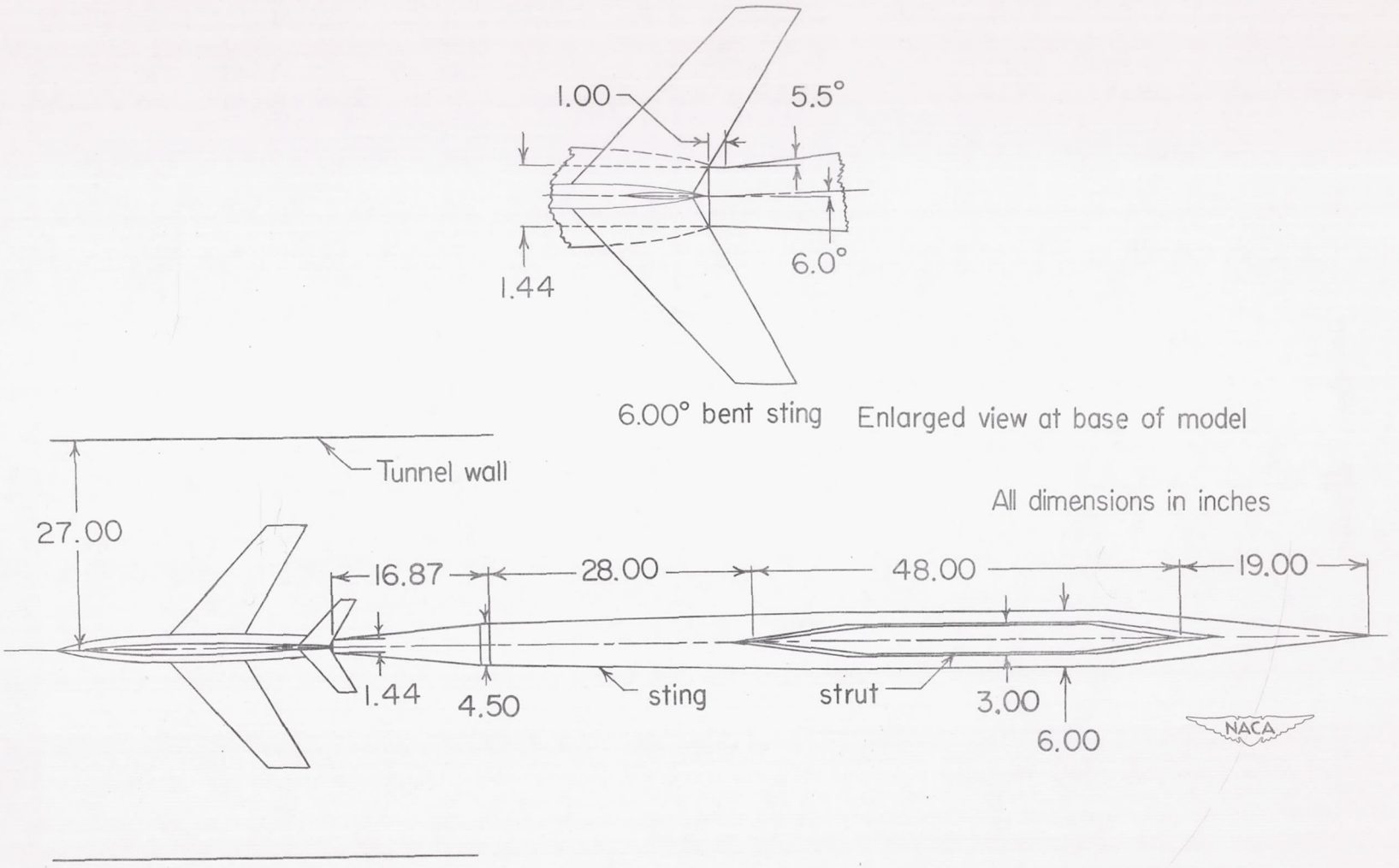

Figure 4.- Details of model support system.

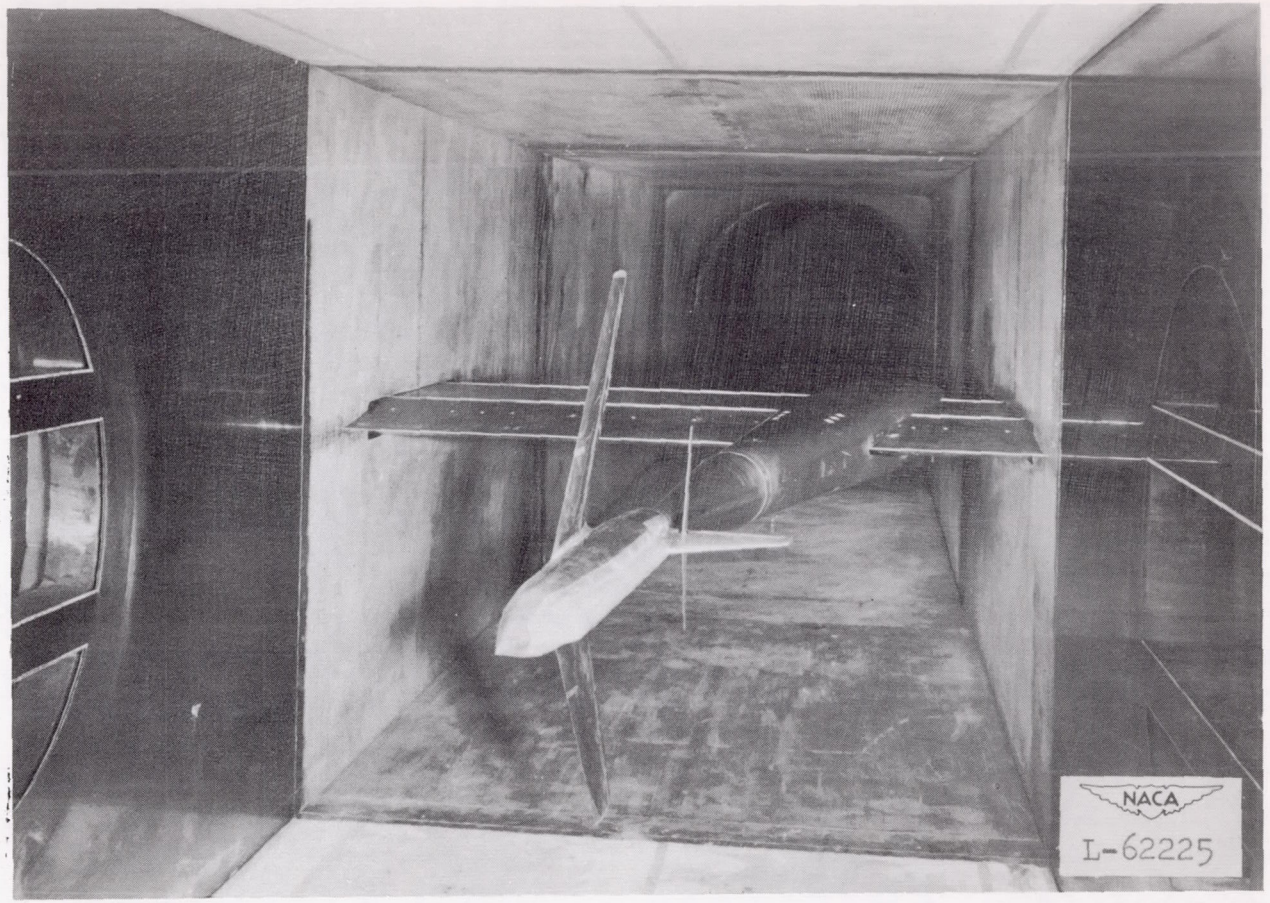

Figure 5.- Model of supersonic aircraft mounted in the Langley 4- by 4-foot supersonic tunnel.

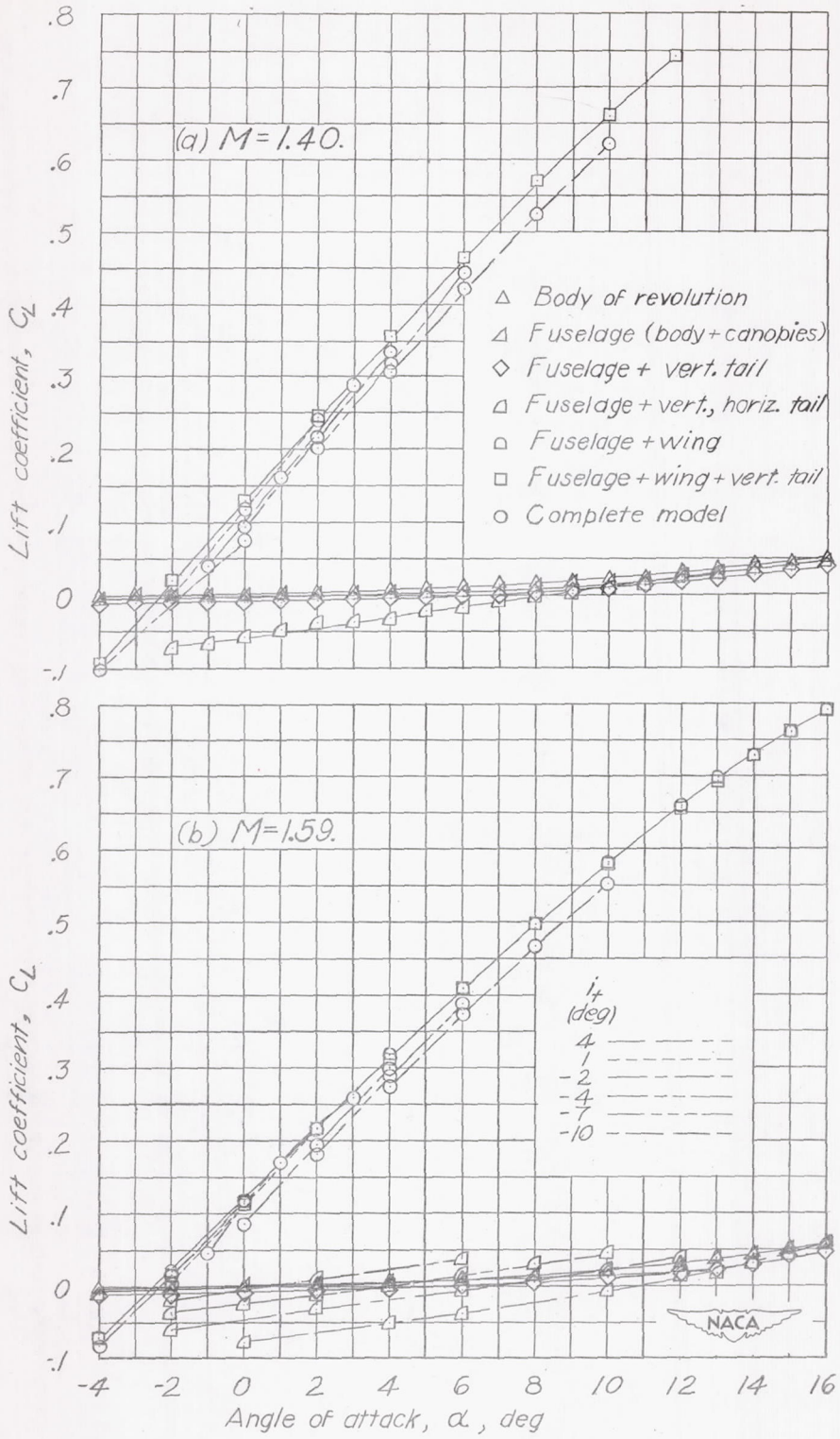

Figure 6.- Variation of lift coefficient with angle of attack for various configurations.

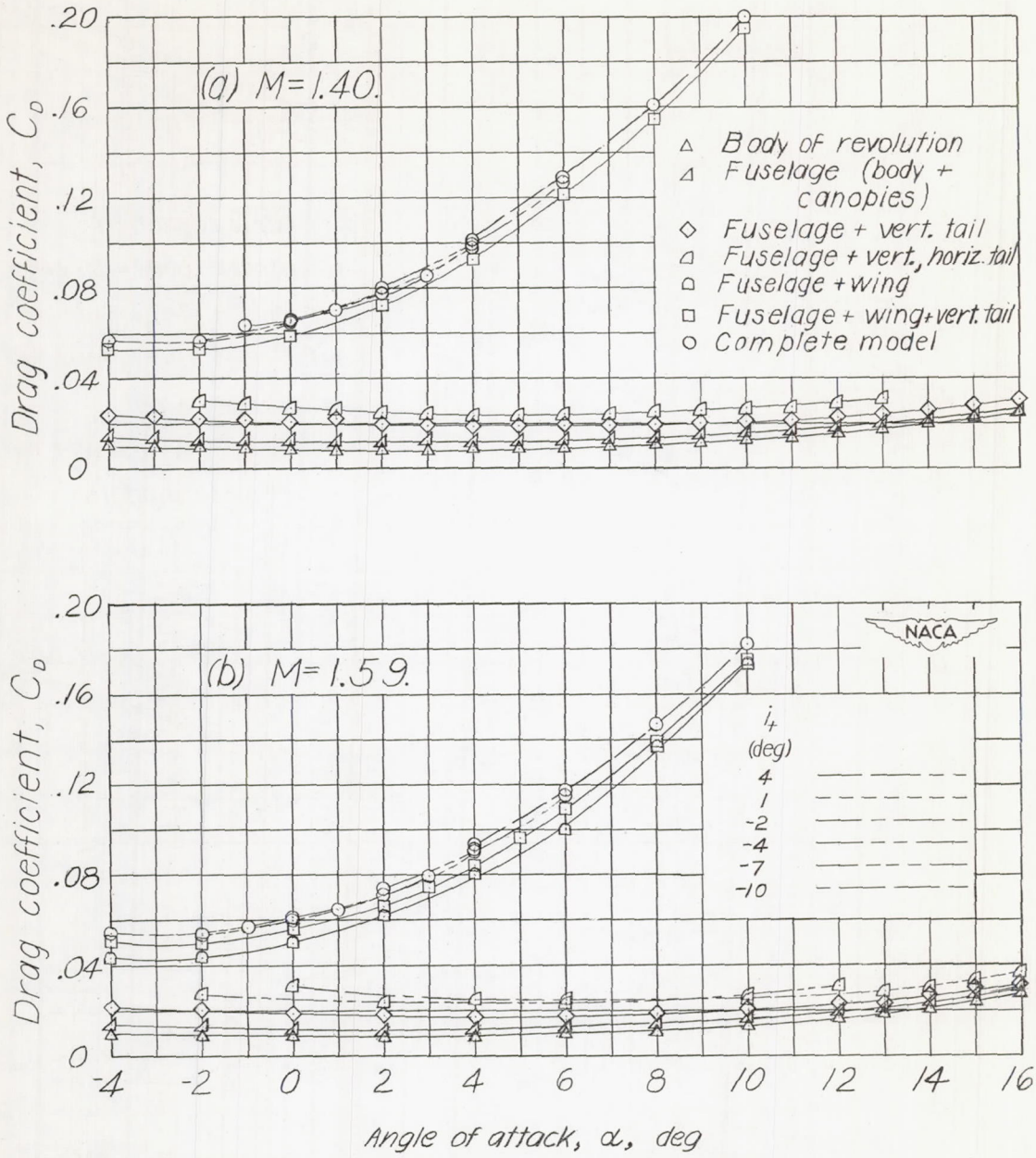

Figure 7.- Variations of drag coefficient with angle of attack for various configurations.

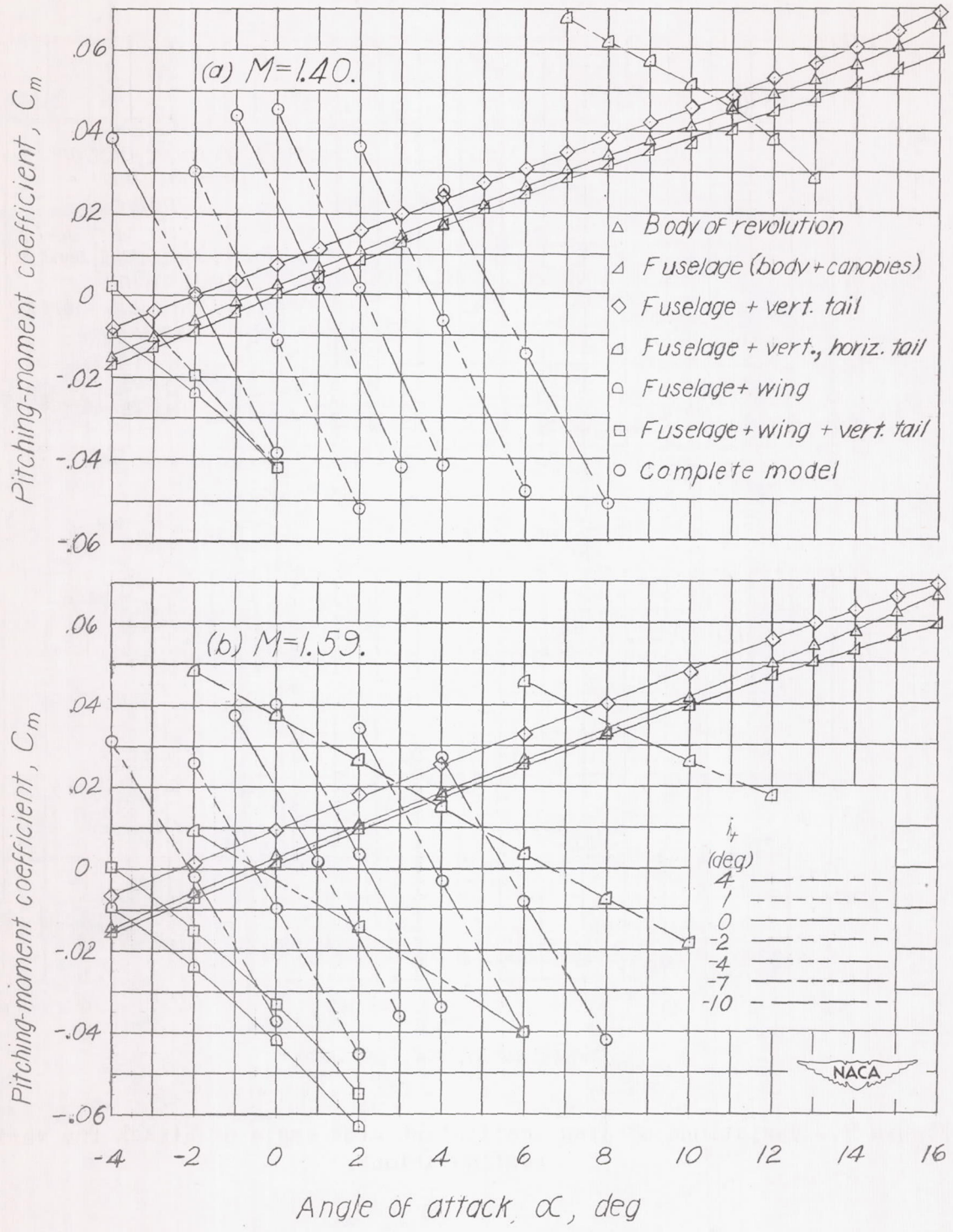

Figure 8.- Variation of pitching-moment coefficient with angle of attack for various configurations.

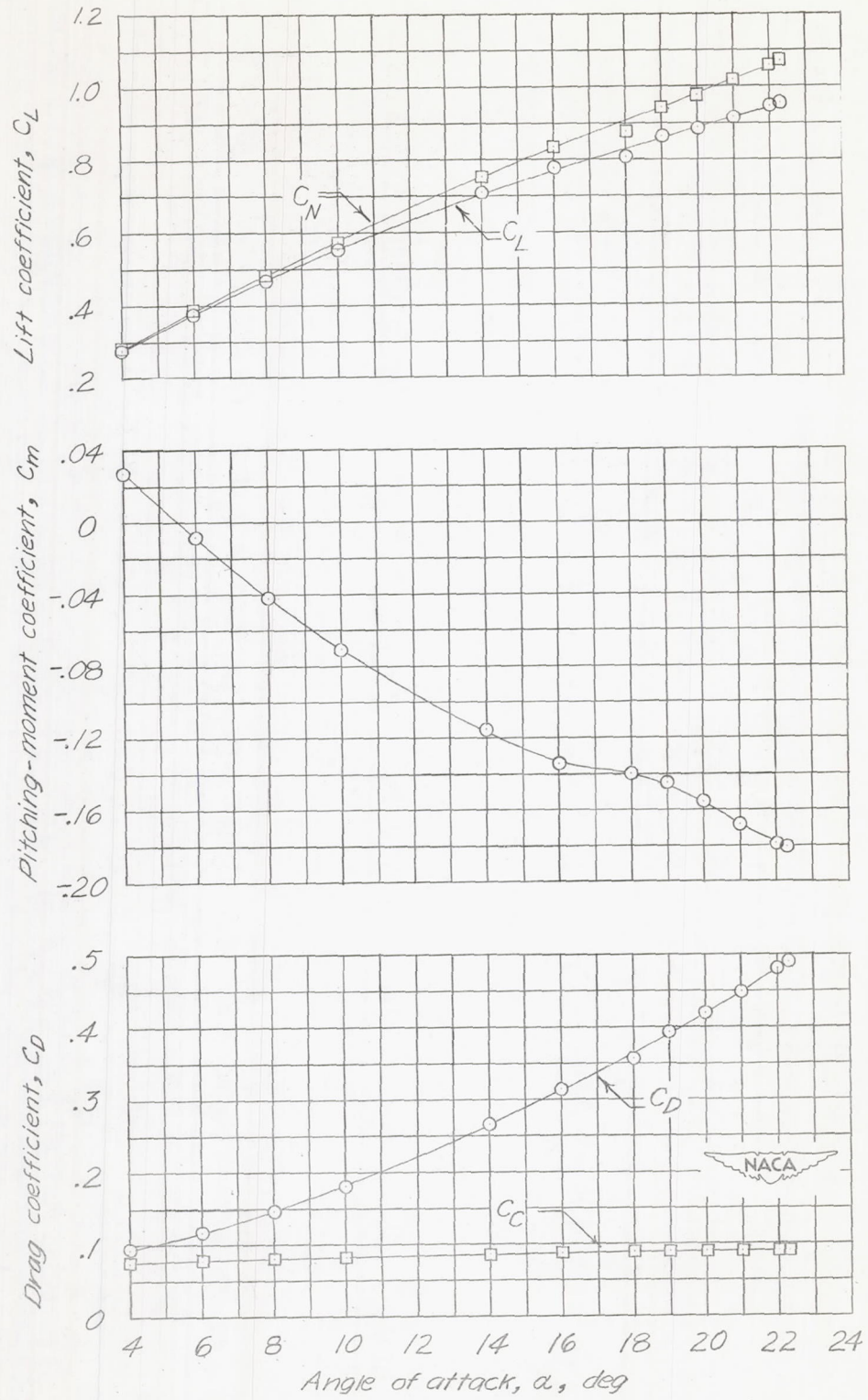

Figure 9.- Longitudinal-force coefficients for complete model up to high angles of attack. M = 1.59; $i_t = -10^\circ$.

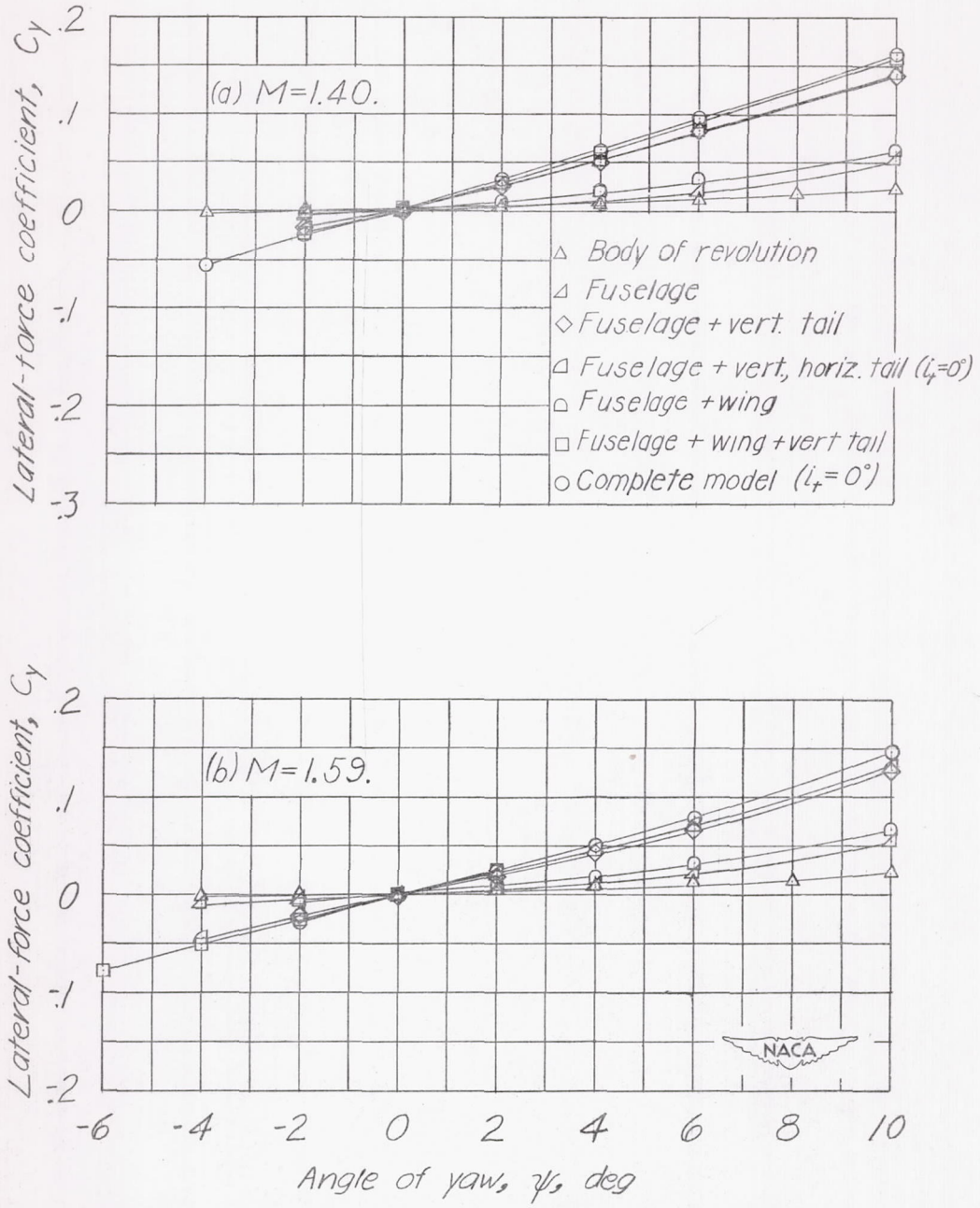

Figure 10.- Variation of lateral-force coefficient with angle of yaw for various configurations. $\alpha = 0^\circ$.

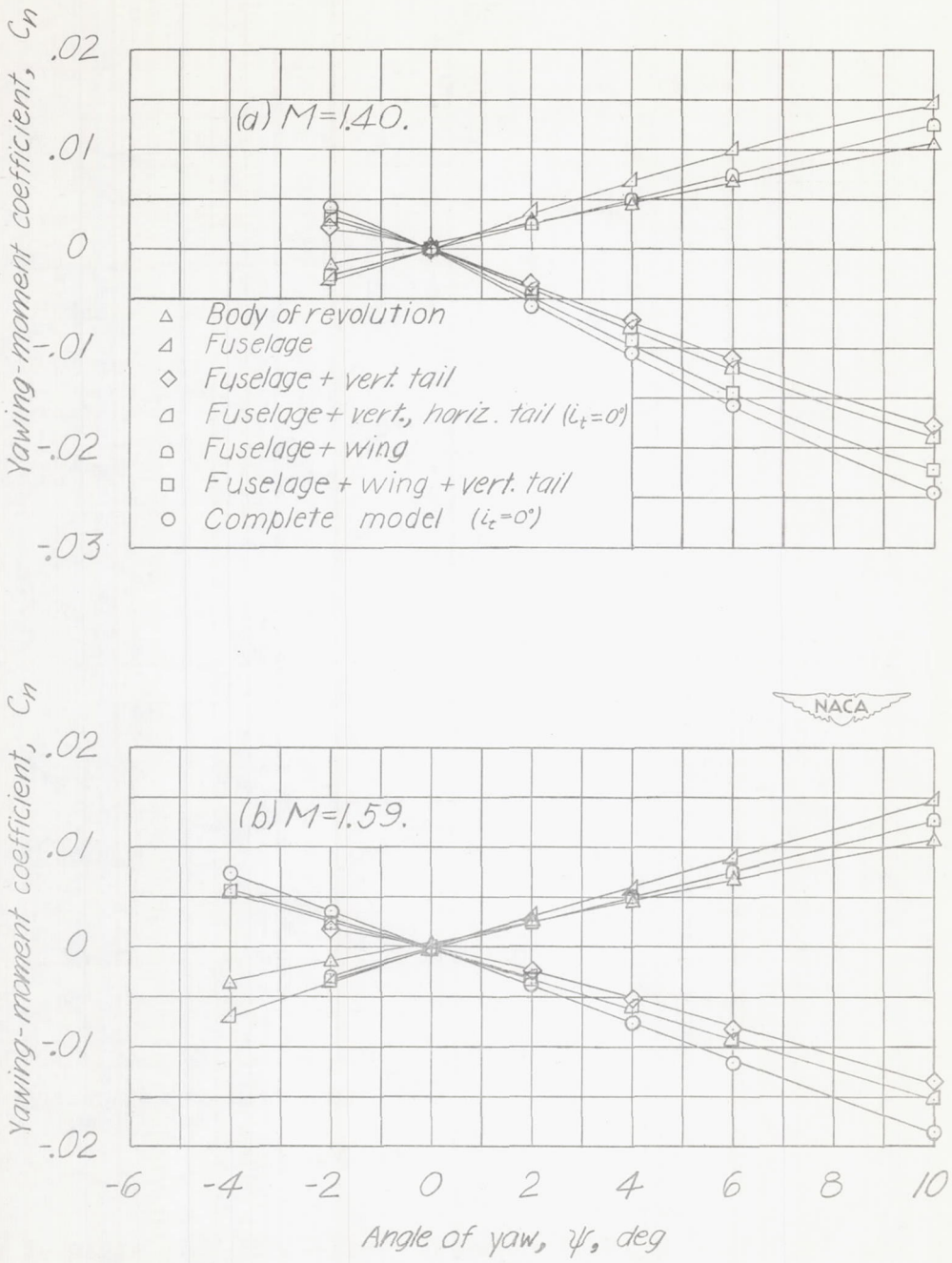

Figure 11.- Variation of yawing-moment coefficient with angle of yaw for various configurations. $\alpha = 0^{\circ}$.

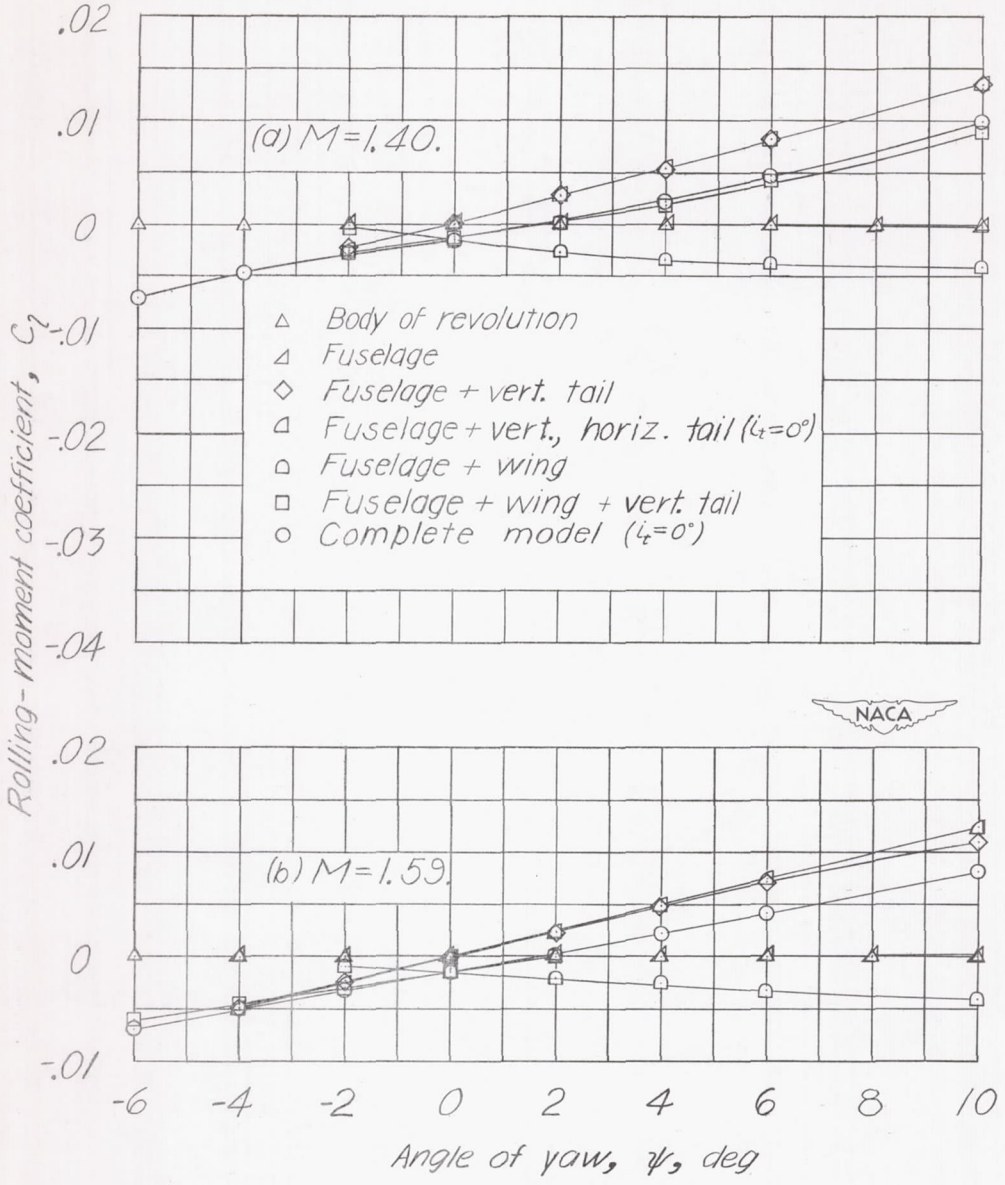

Figure 12.- Variation of rolling-moment coefficient with angle of yaw for various configurations. $\alpha = 0^{\circ}$.

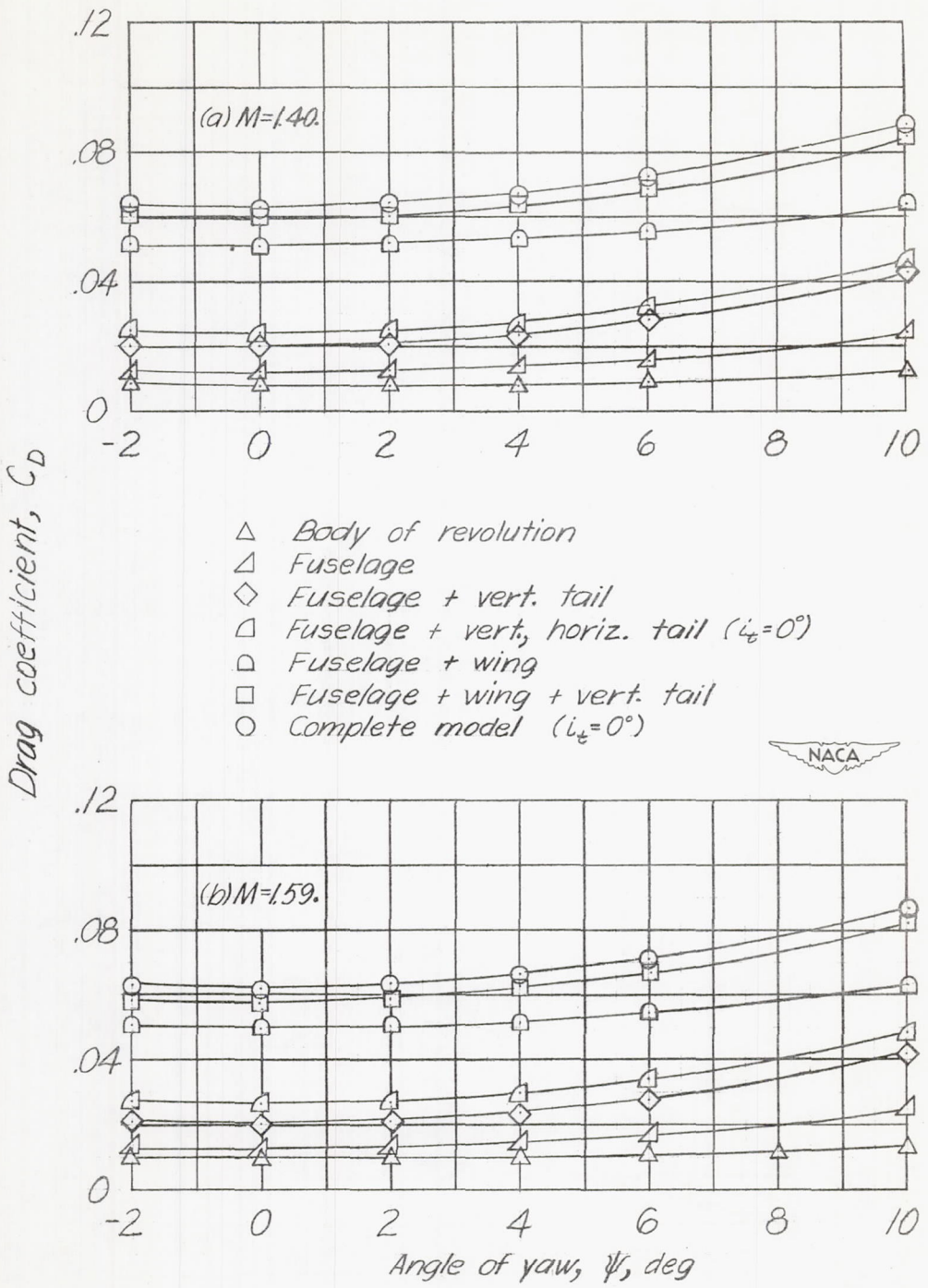

Figure 13.- Variation of drag coefficient with angle of yaw for various configurations. $\alpha = 0^\circ$.

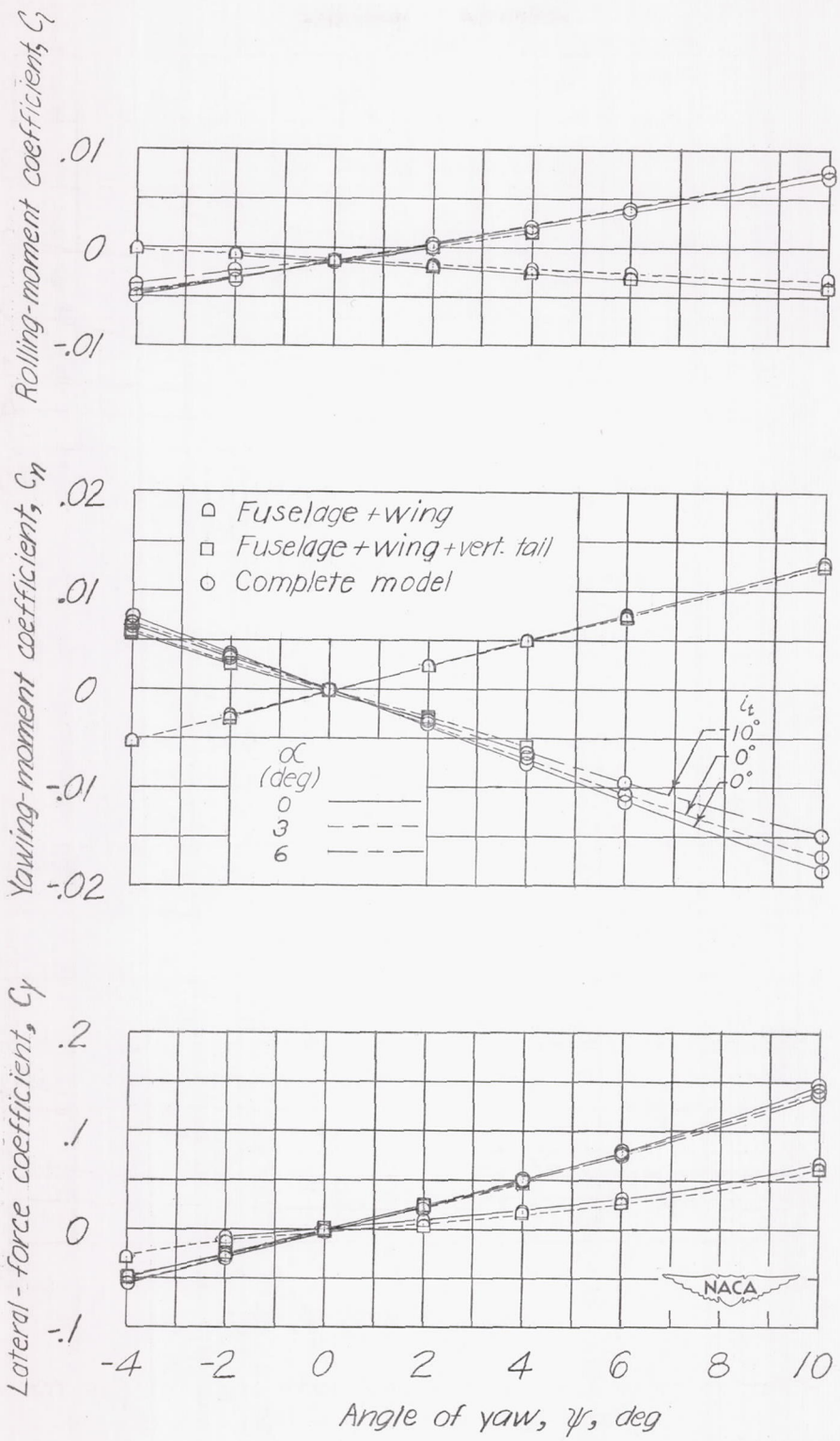

Figure 14.- Variation of lateral coefficients with yaw angle for three angles of attack. M = 1.59.

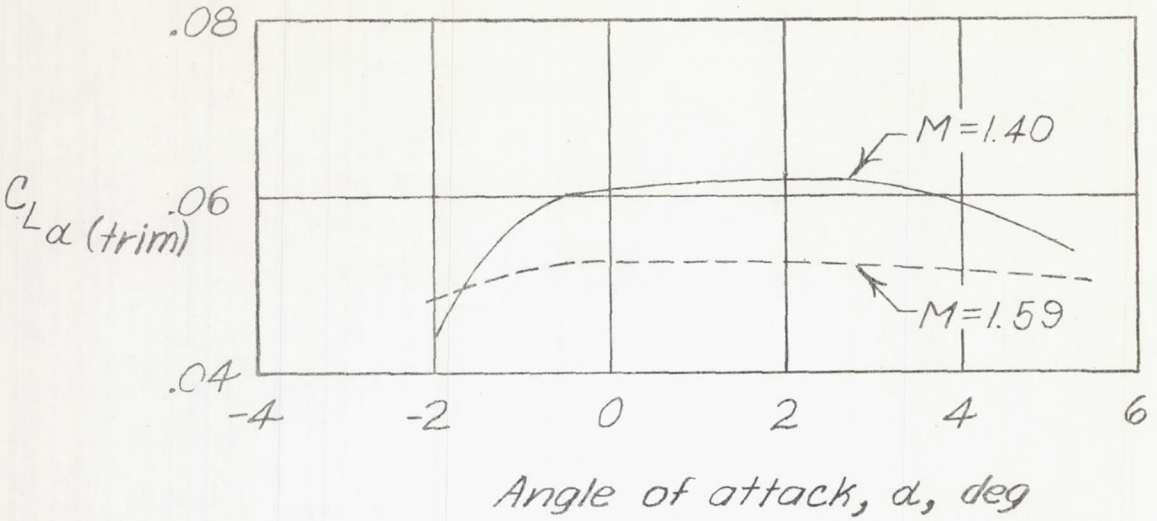

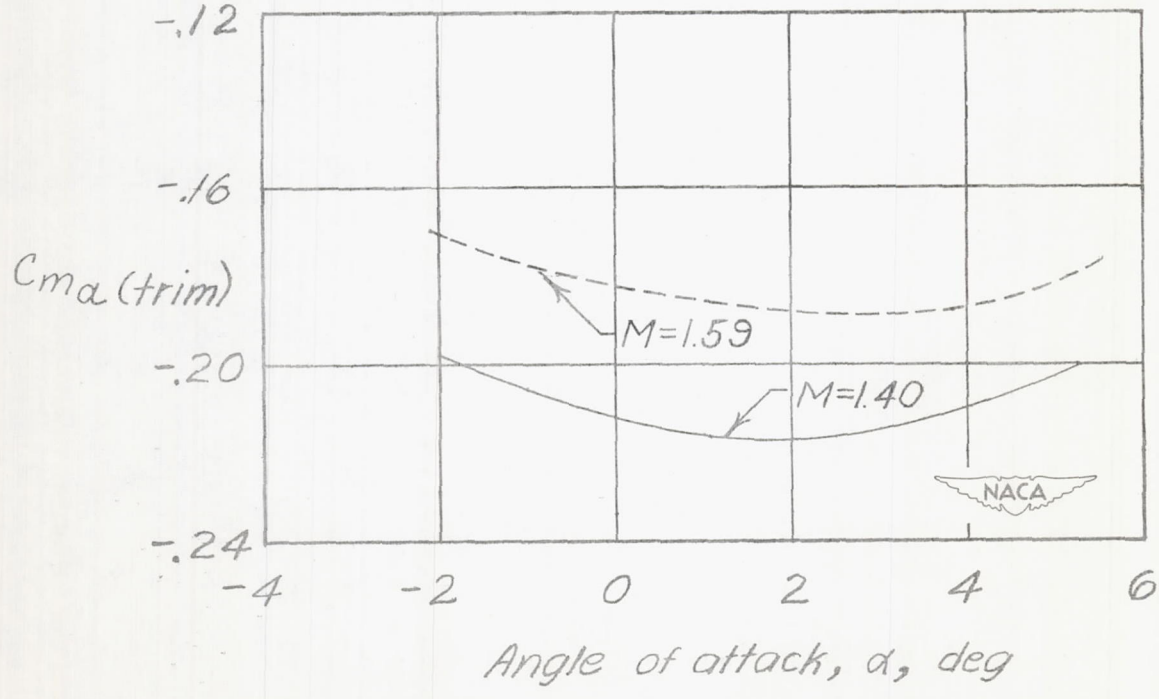

Figure 15.- Lift-curve and moment-curve slopes for the complete model.

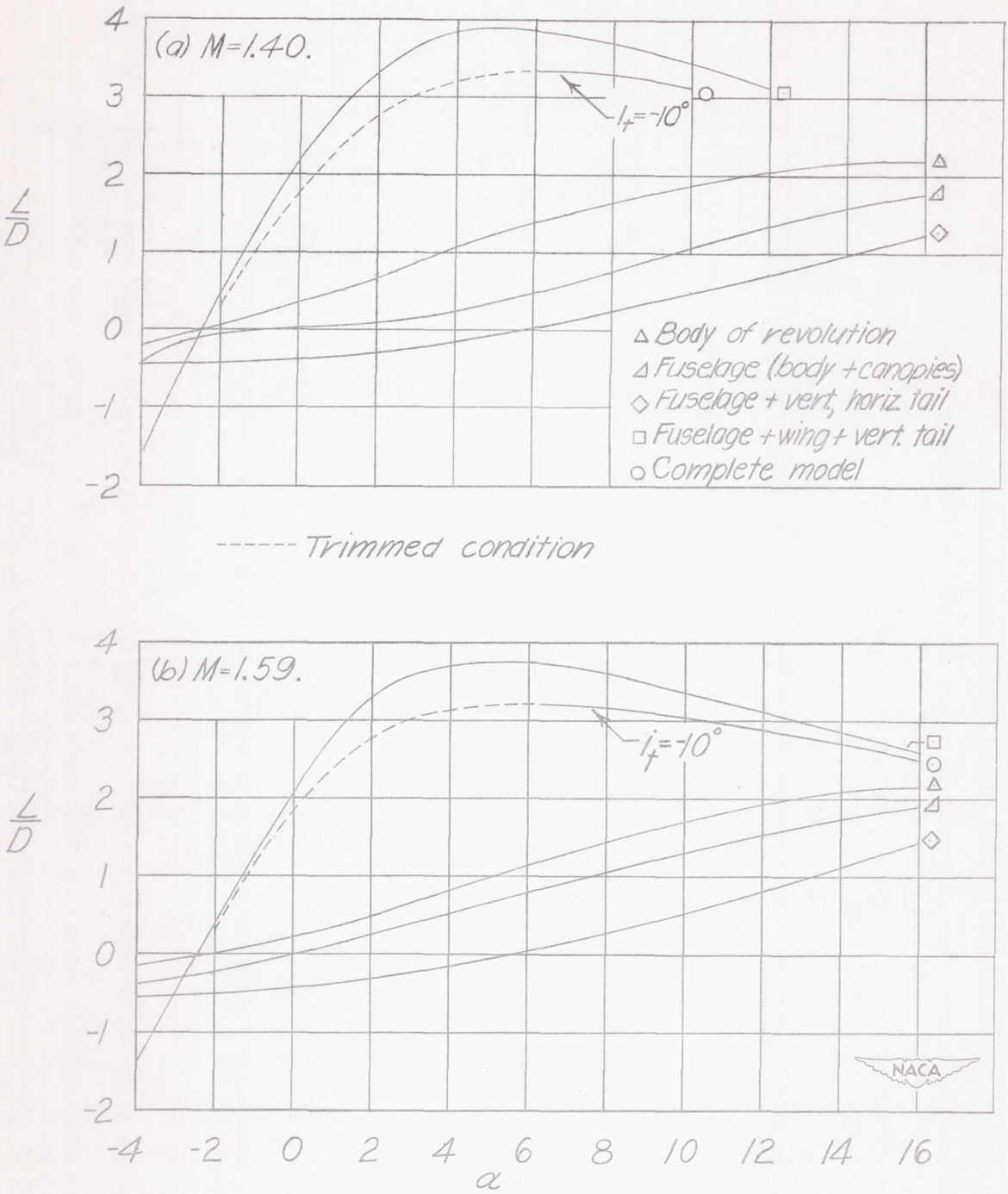

Figure 16.- Lift-drag ratios for various configurations.

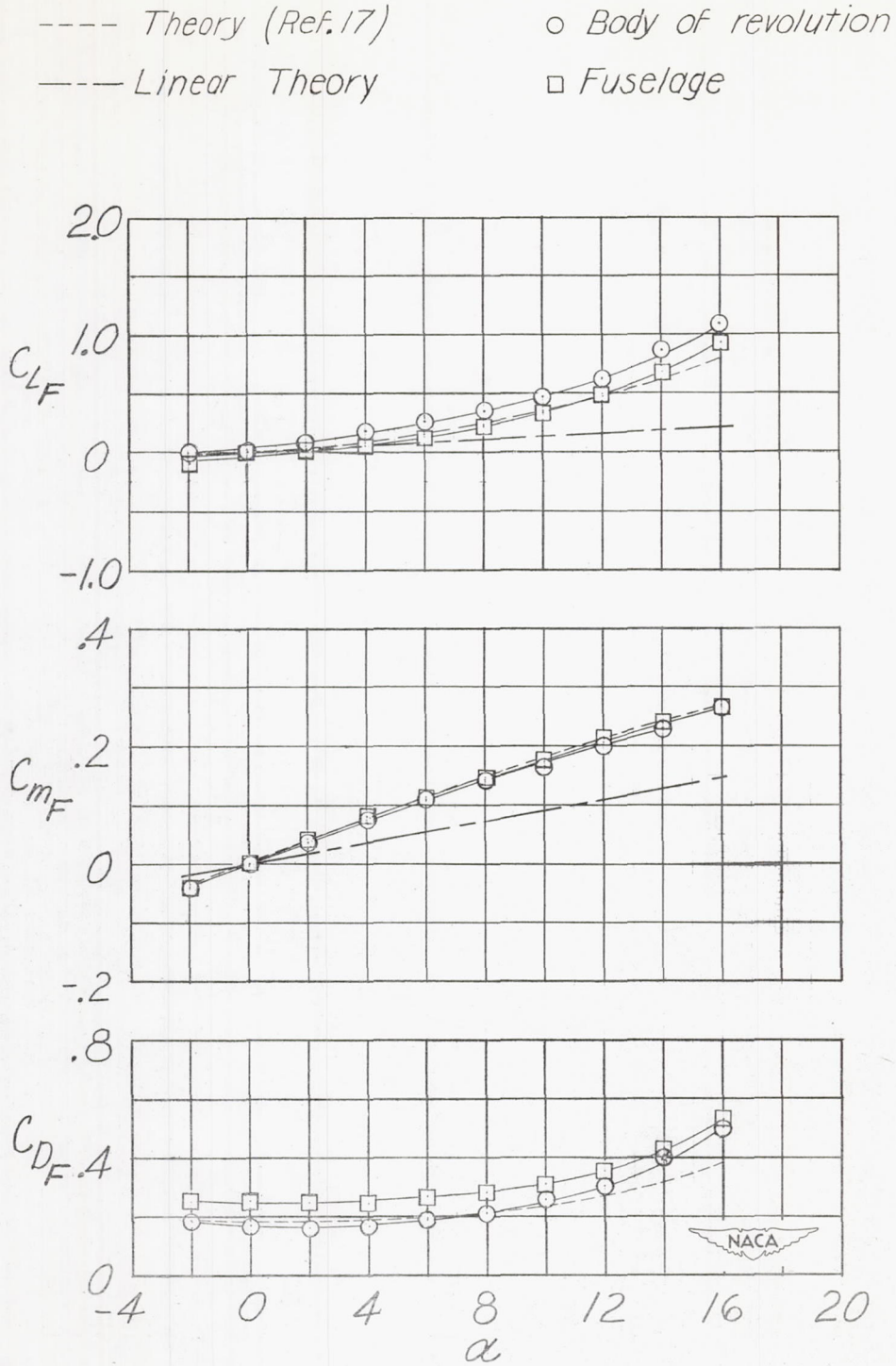

(a) M = 1.40.

Figure 17.- Aerodynamic characteristics of body of revolution and fuselage, based on body frontal area.

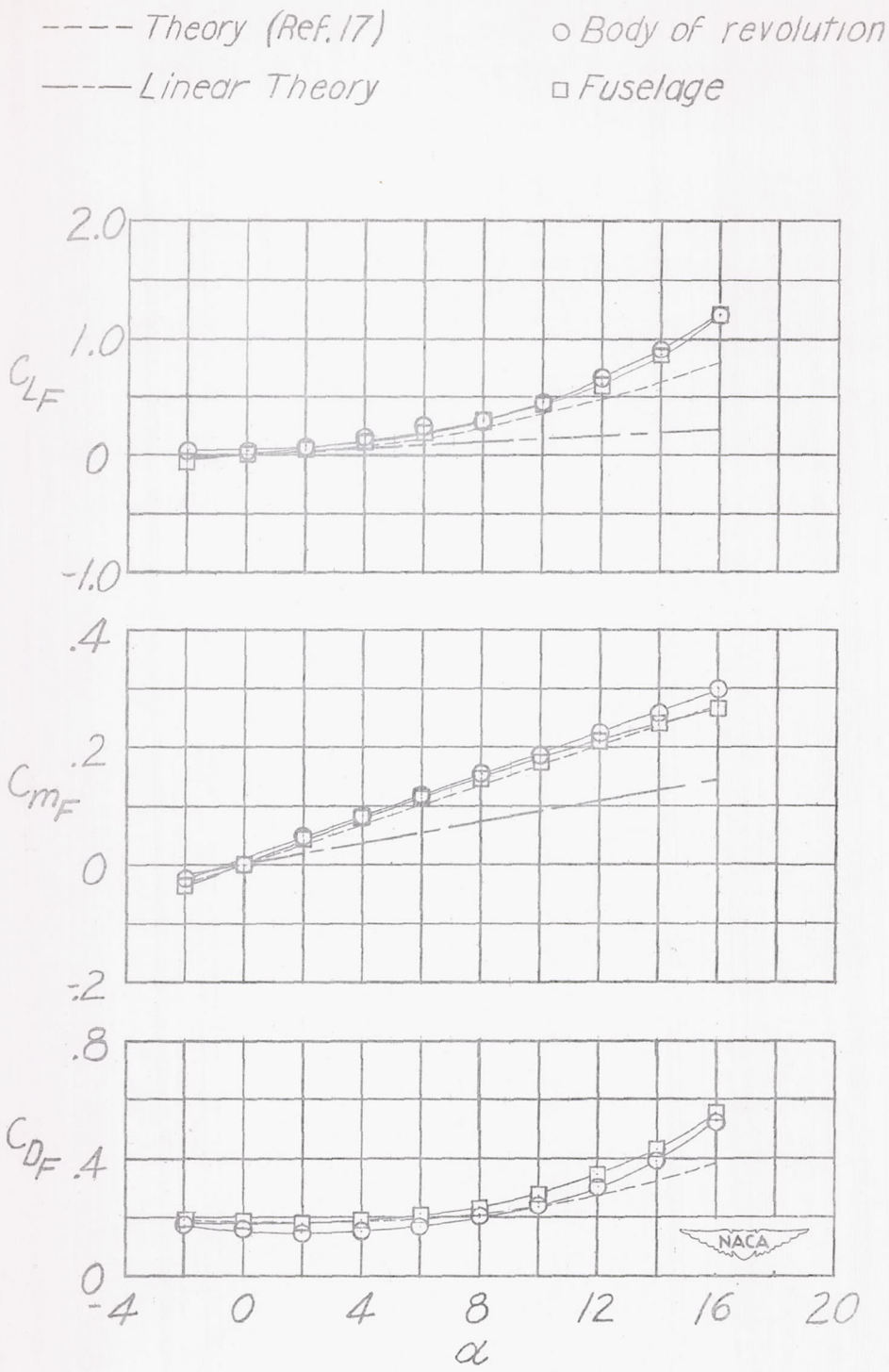

(b) M = 1.59.

Figure 17.- Concluded.

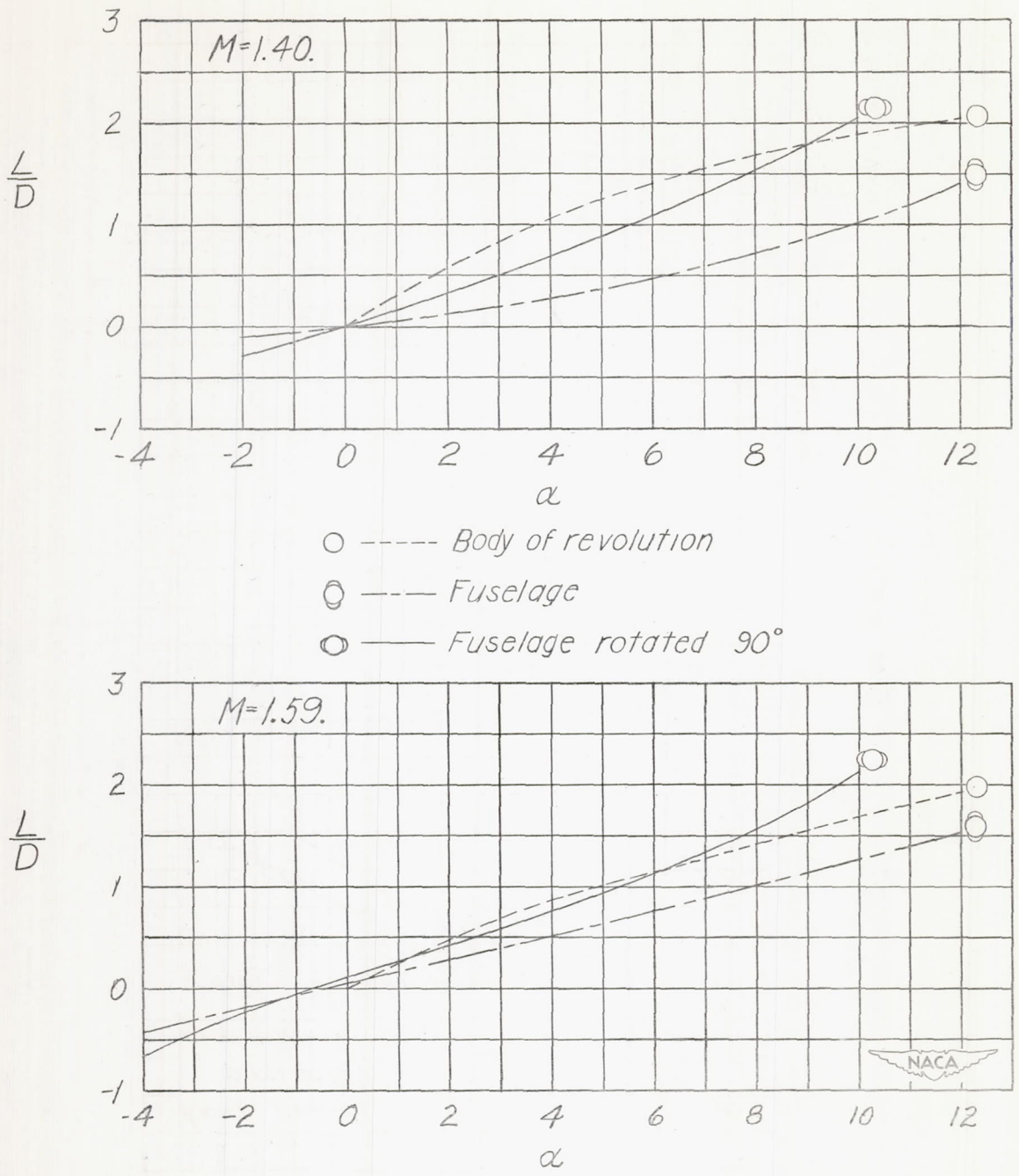

Figure 18.- Lift-drag ratios for body of revolution, fuselage, and fuselage rotated 90°.

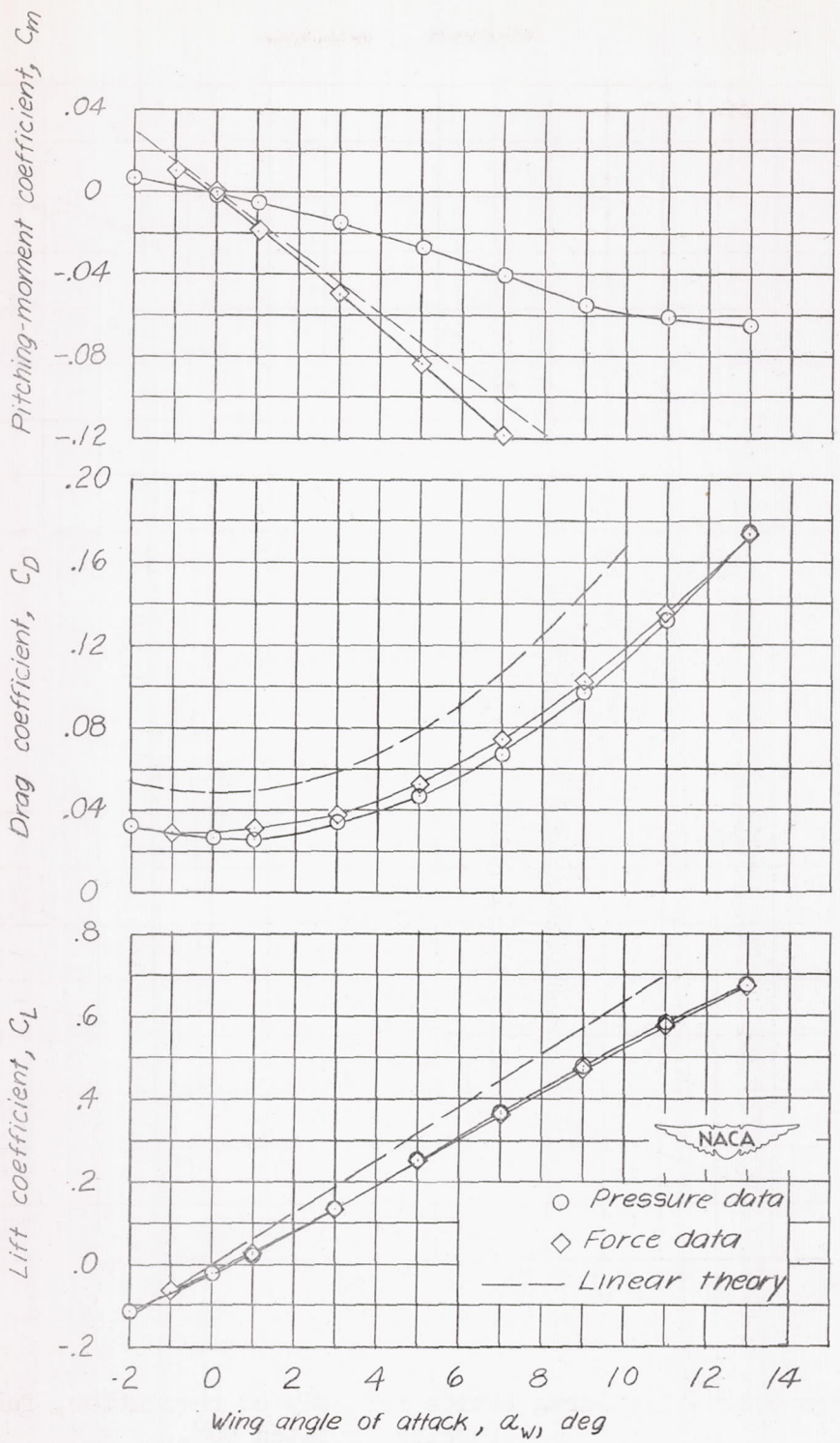

(a) M = 1.40.

Figure 19.- Aerodynamic characteristics of wing.

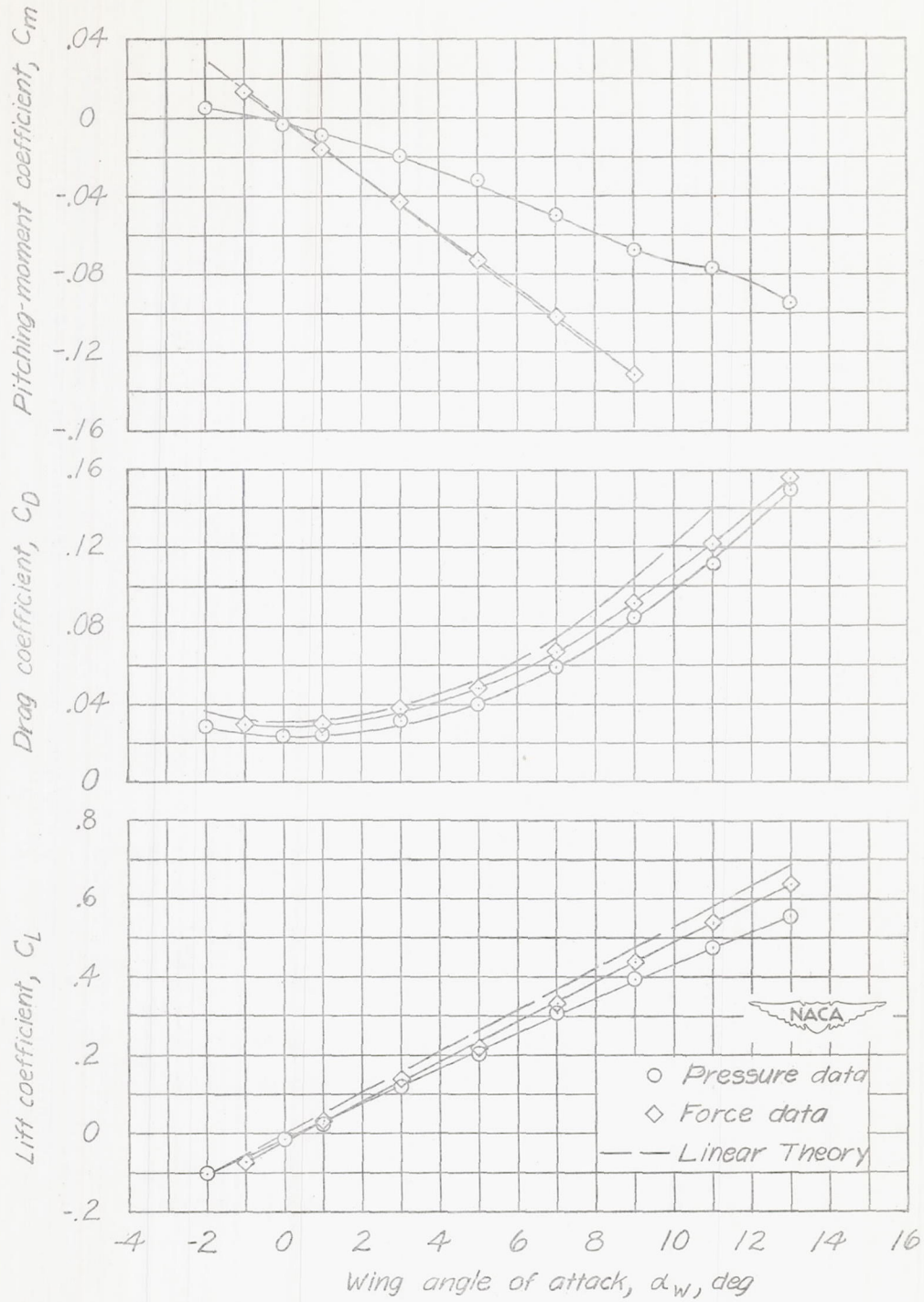

(b) M = 1.59.

Figure 19.- Concluded.

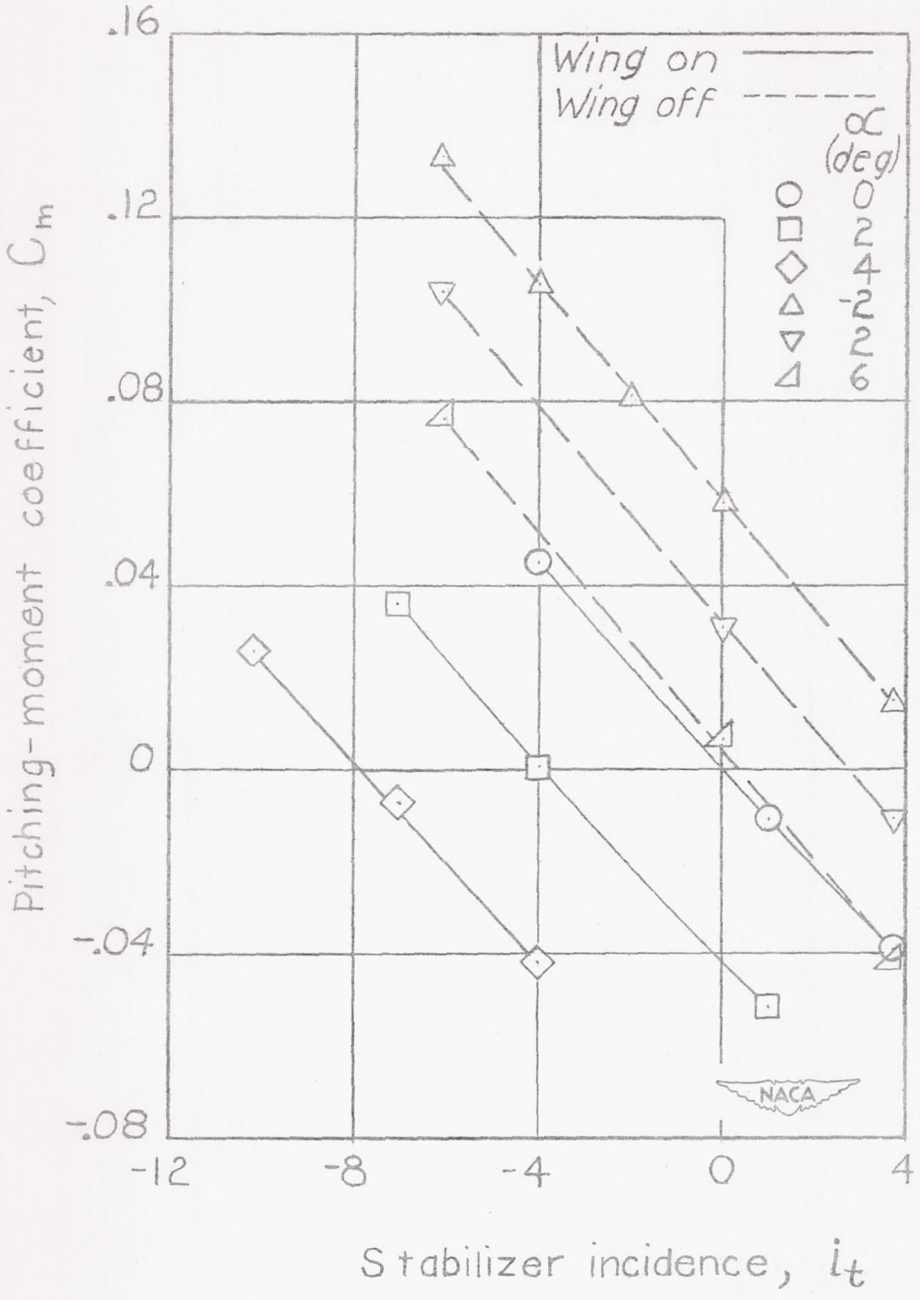

(a) M = 1.40.

Figure 20.- Variation of pitching-moment coefficient with stabilizer incidence.

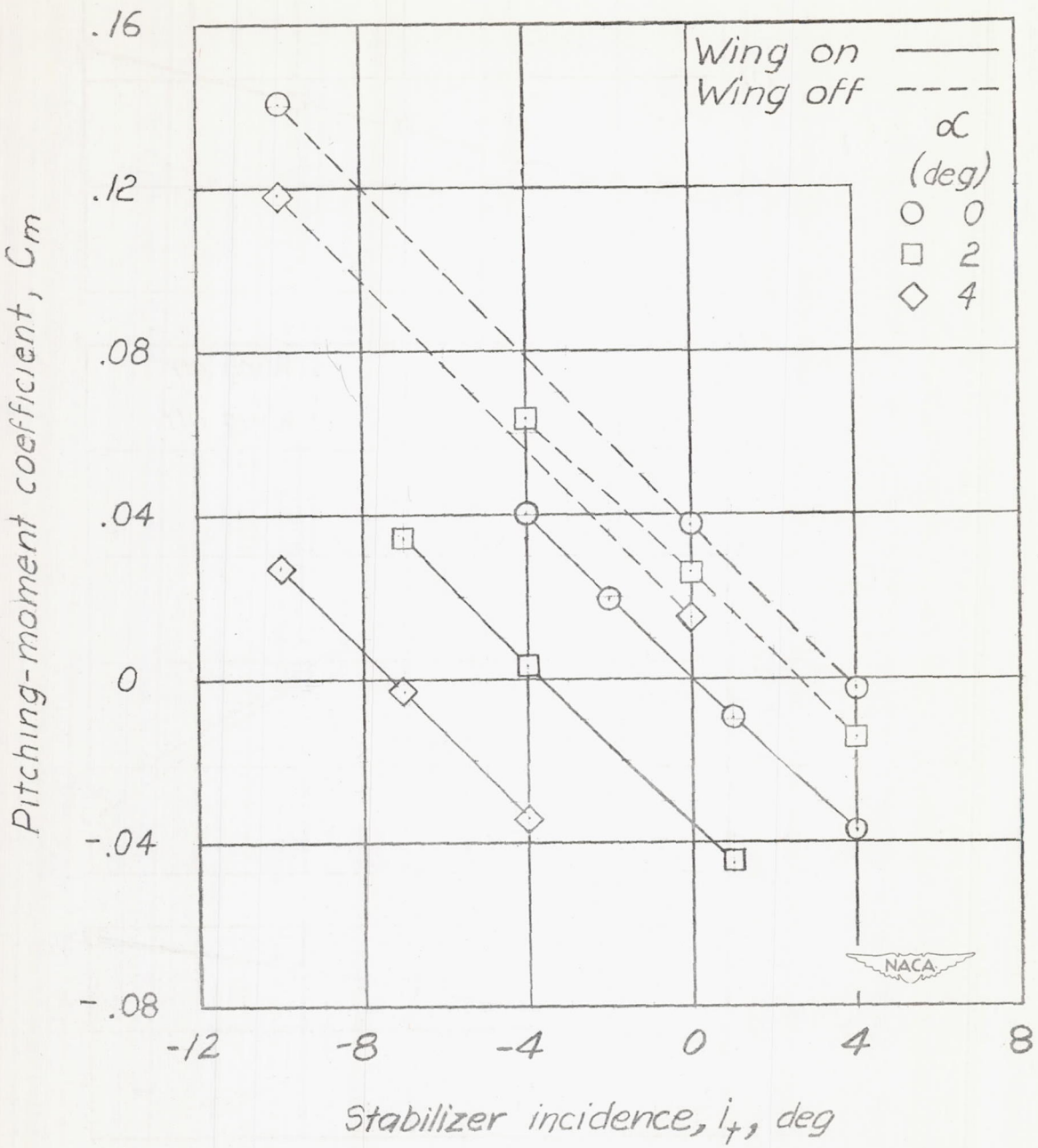

(b) M = 1.59.

Figure 20.- Concluded.

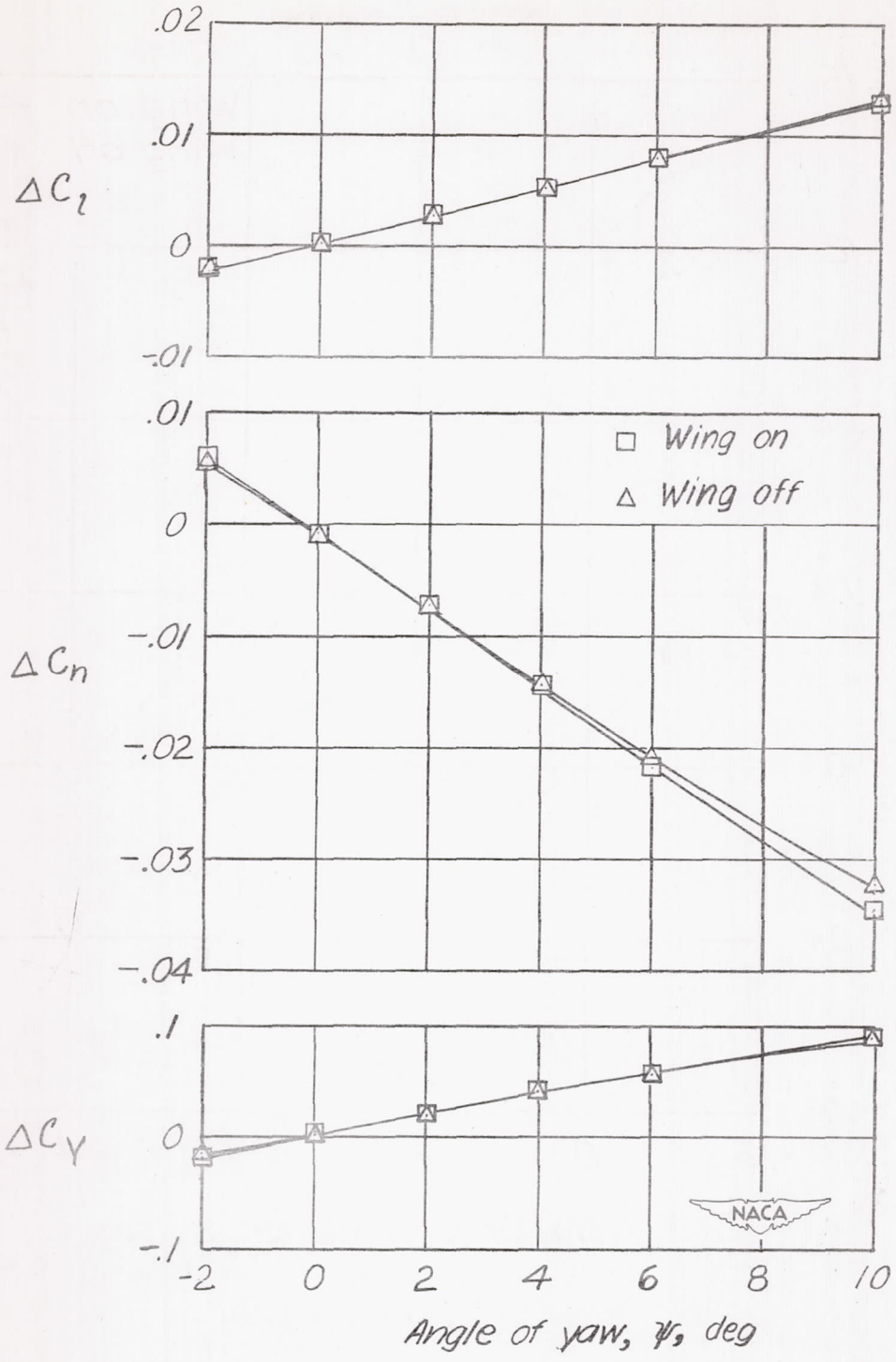

(a) M = 1.40.

Figure 21.- Effect of wing on the incremental lateral coefficients produced by the vertical tail. $\alpha = 0^{\circ}$.

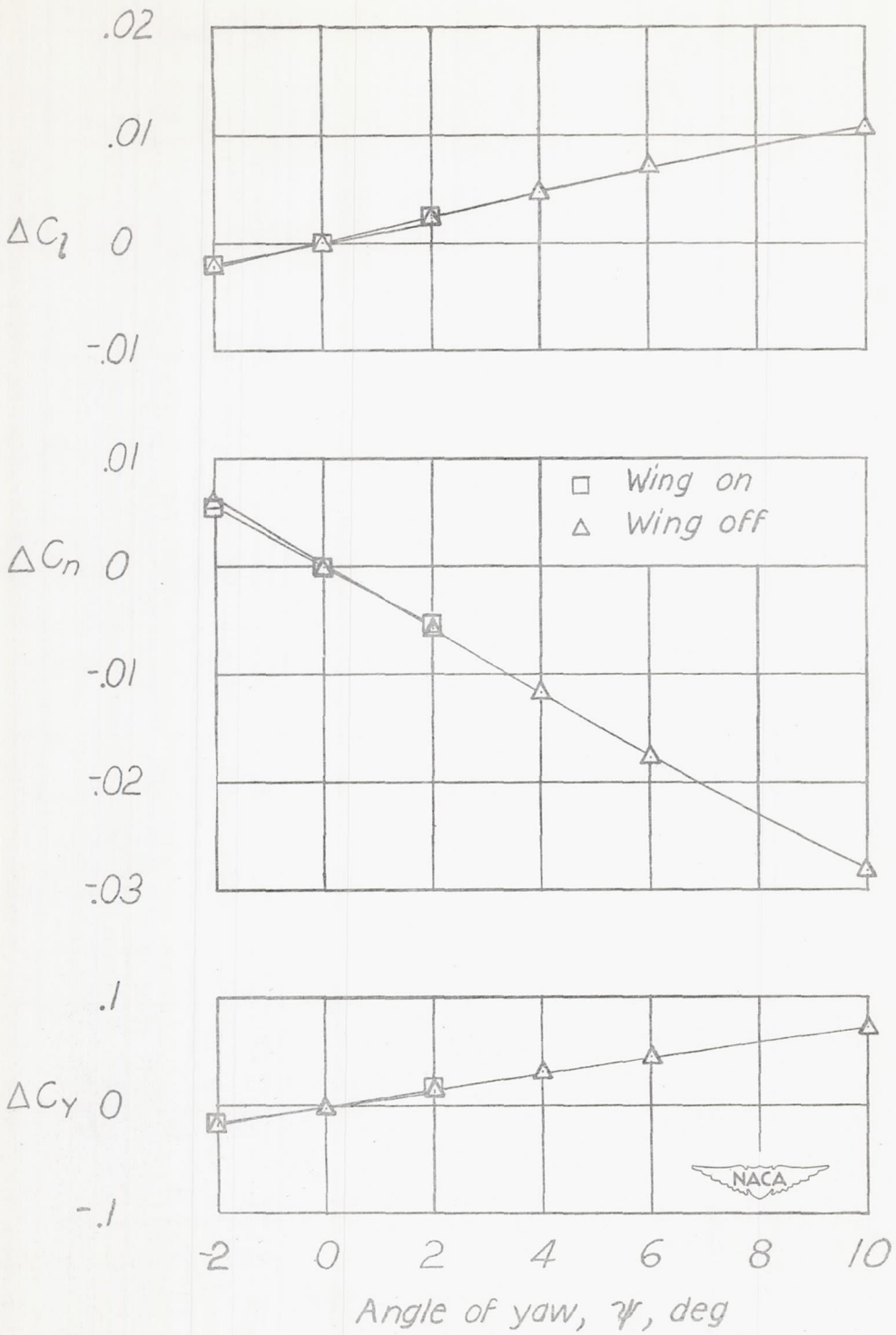

(b) M = 1.59.

Figure 21.- Concluded.

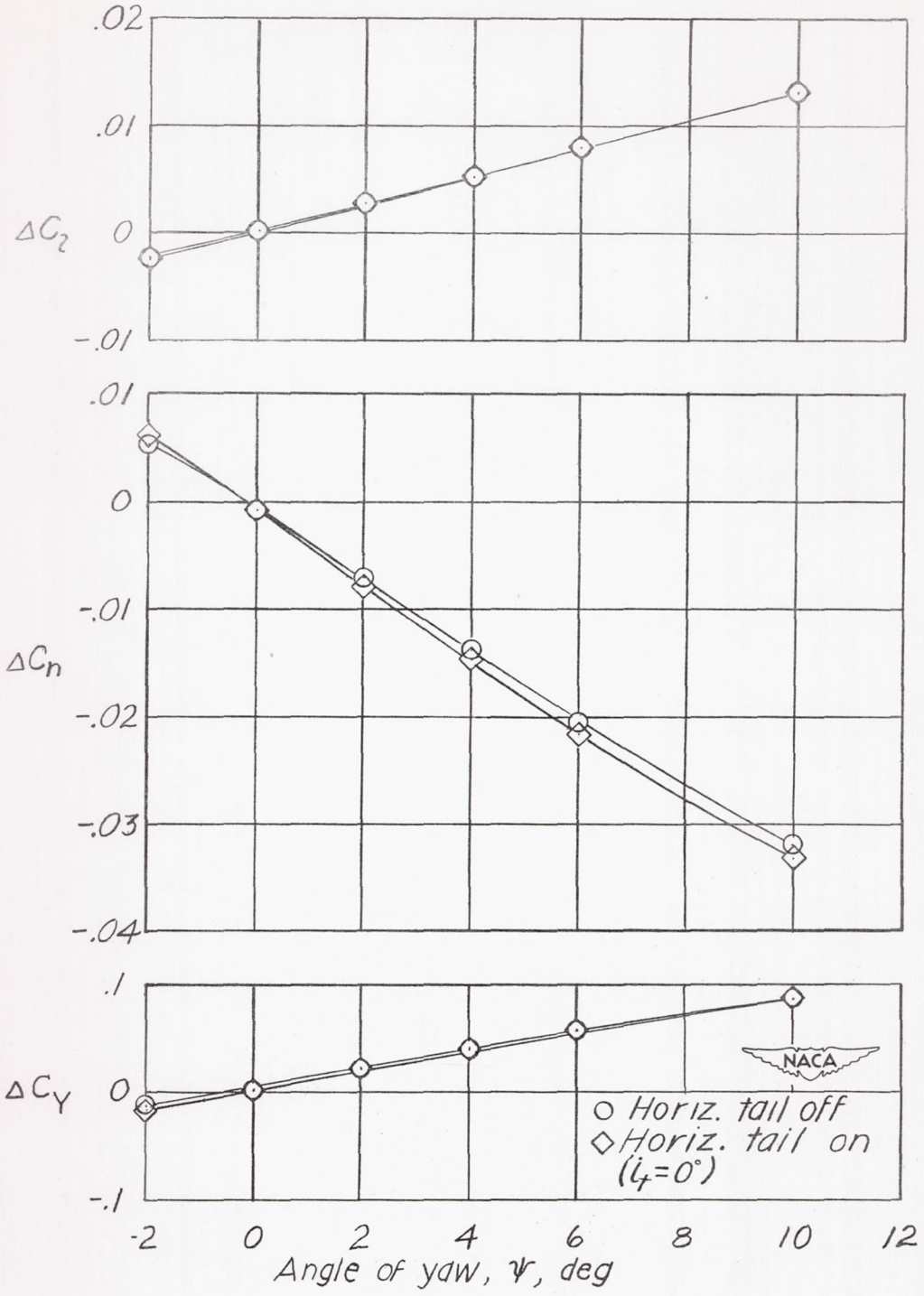

(a) M = 1.40.

Figure 22.- Effect of horizontal tail on the incremental lateral coefficients produced by the vertical tail. $\alpha = 0^{\circ}$.

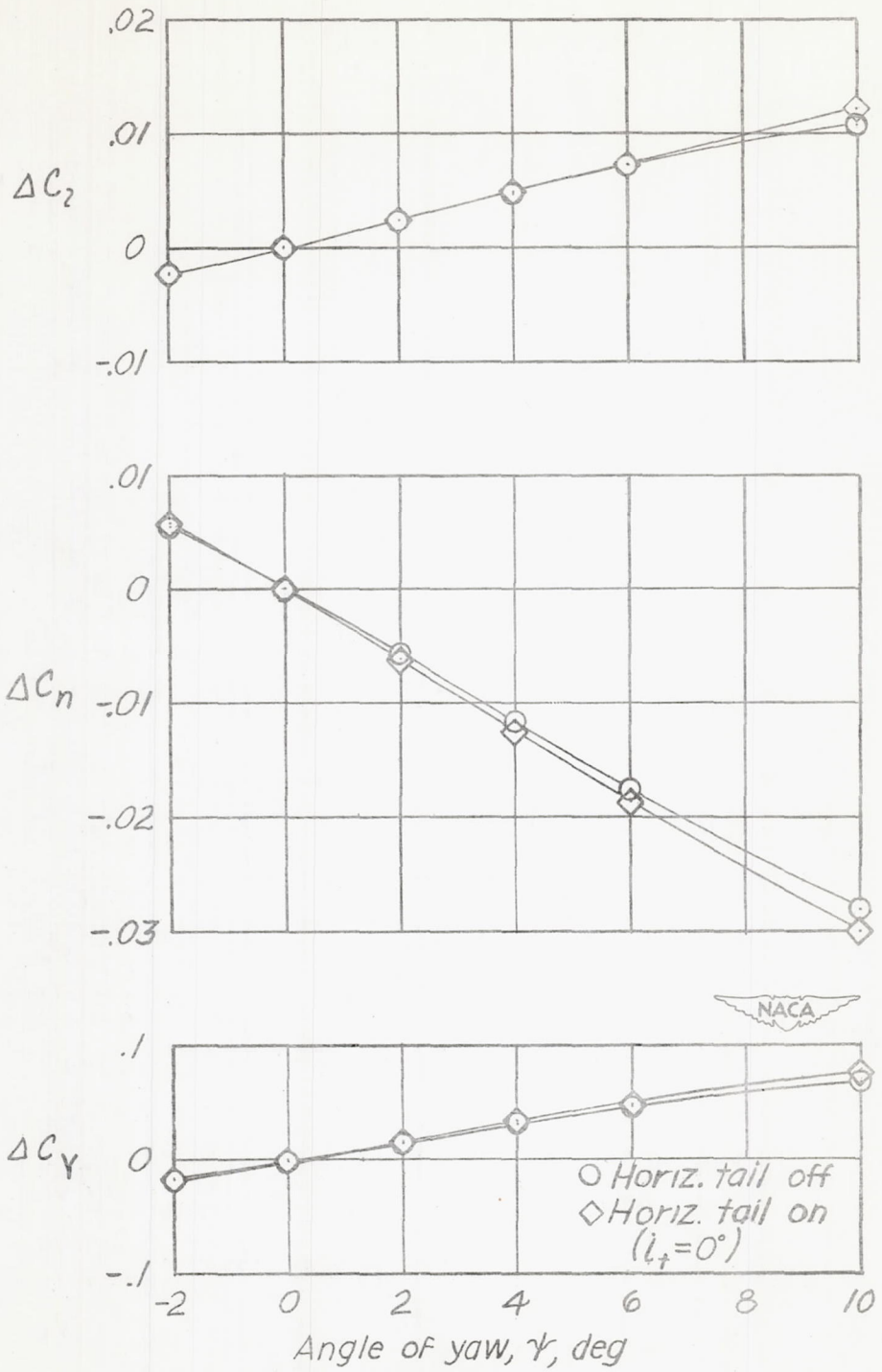

(b) M = 1.59.

Figure 22.- Concluded.

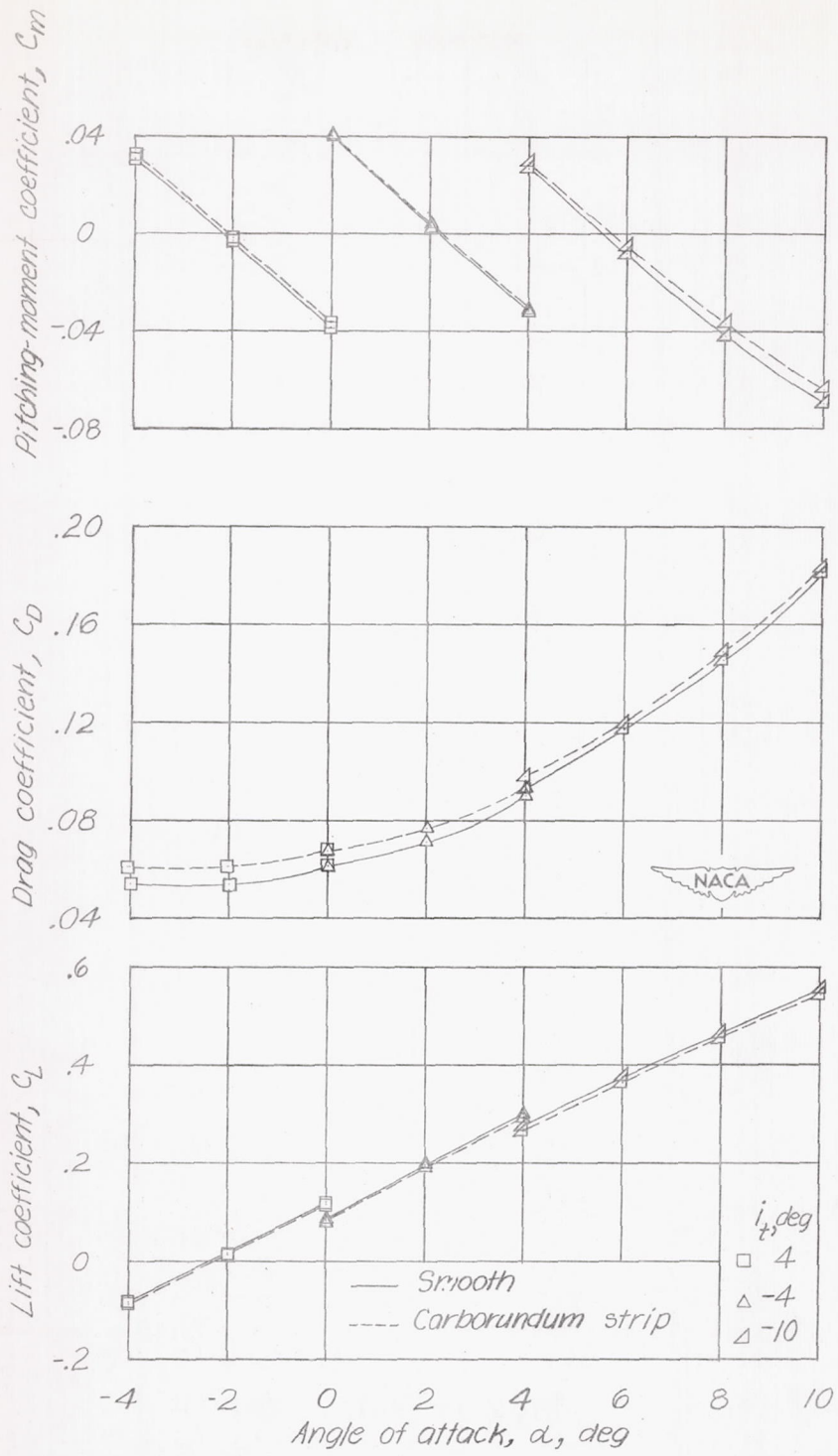

Figure 23.- Comparison of longitudinal characteristics of complete model smooth and with $\frac{1}{8}$-inch carborundum strip at 10 percent from leading edge of all surfaces. M = 1.59.

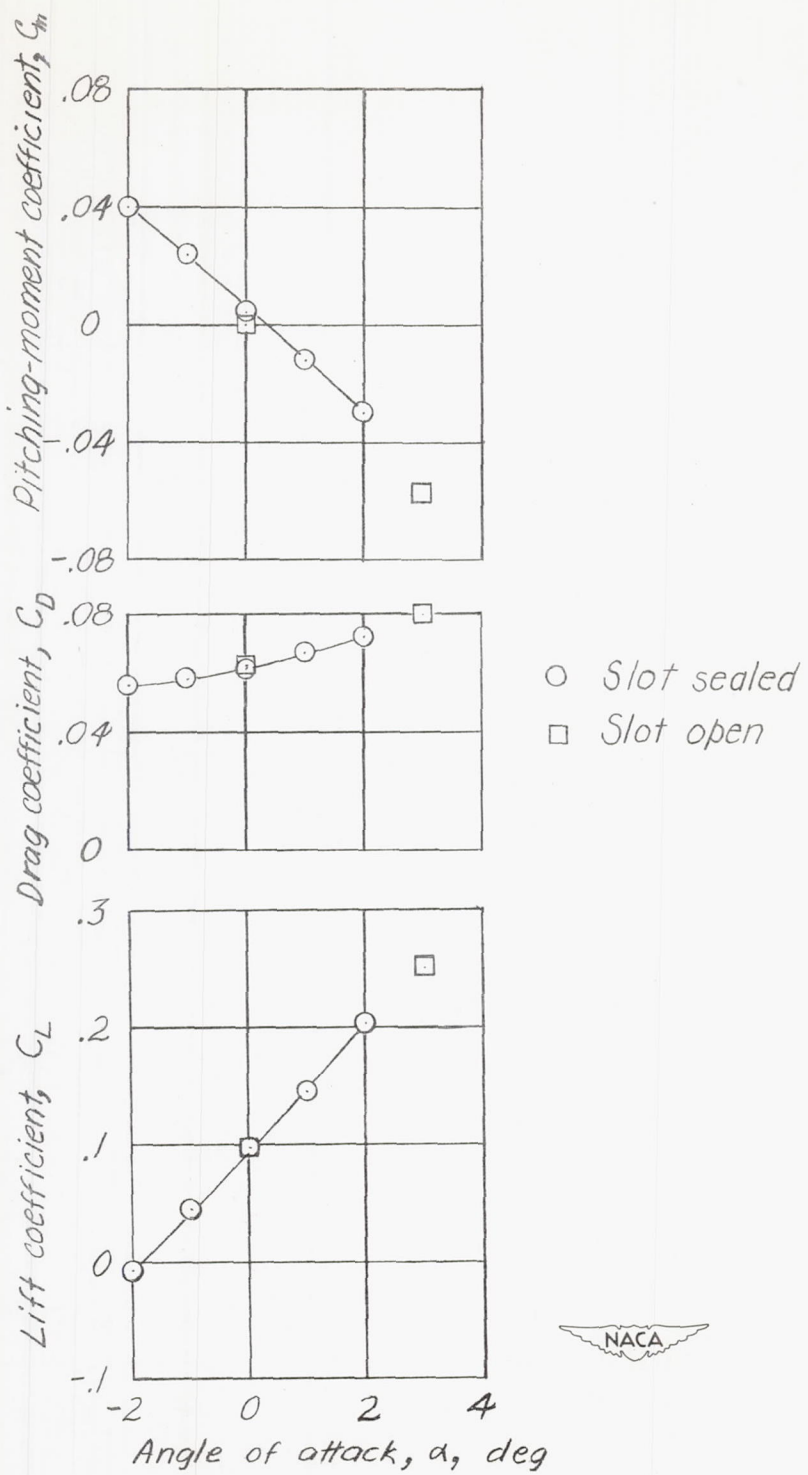

(a) Longitudinal characteristics.

Figure 24.- Effect of sealing slot in vertical tail on the aerodynamic characteristics of the complete model. M = 1.59; $i_t = 0^\circ$.

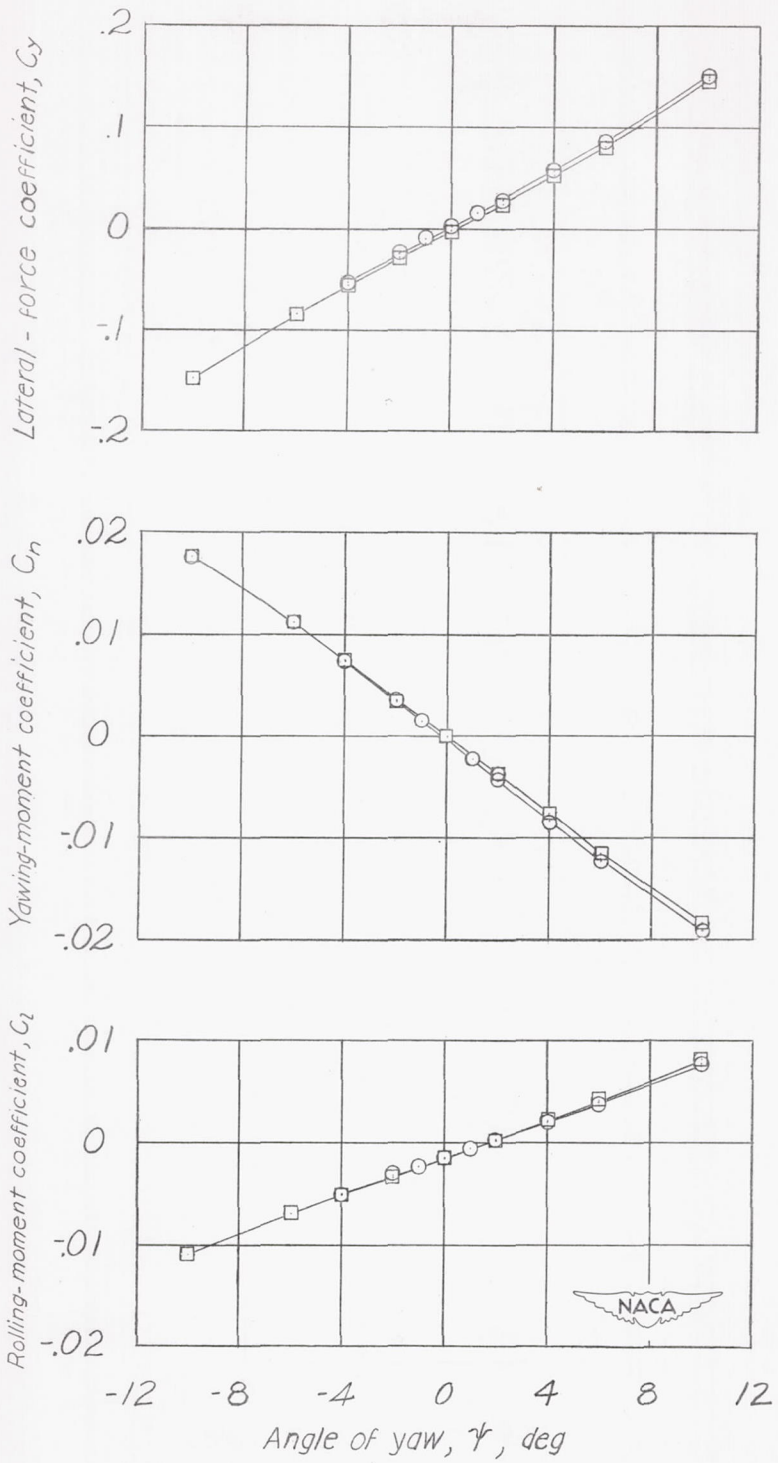

(b) Lateral characteristics.
$\alpha = 0$; $i_t = 0^\circ$.

Figure 24.- Concluded.

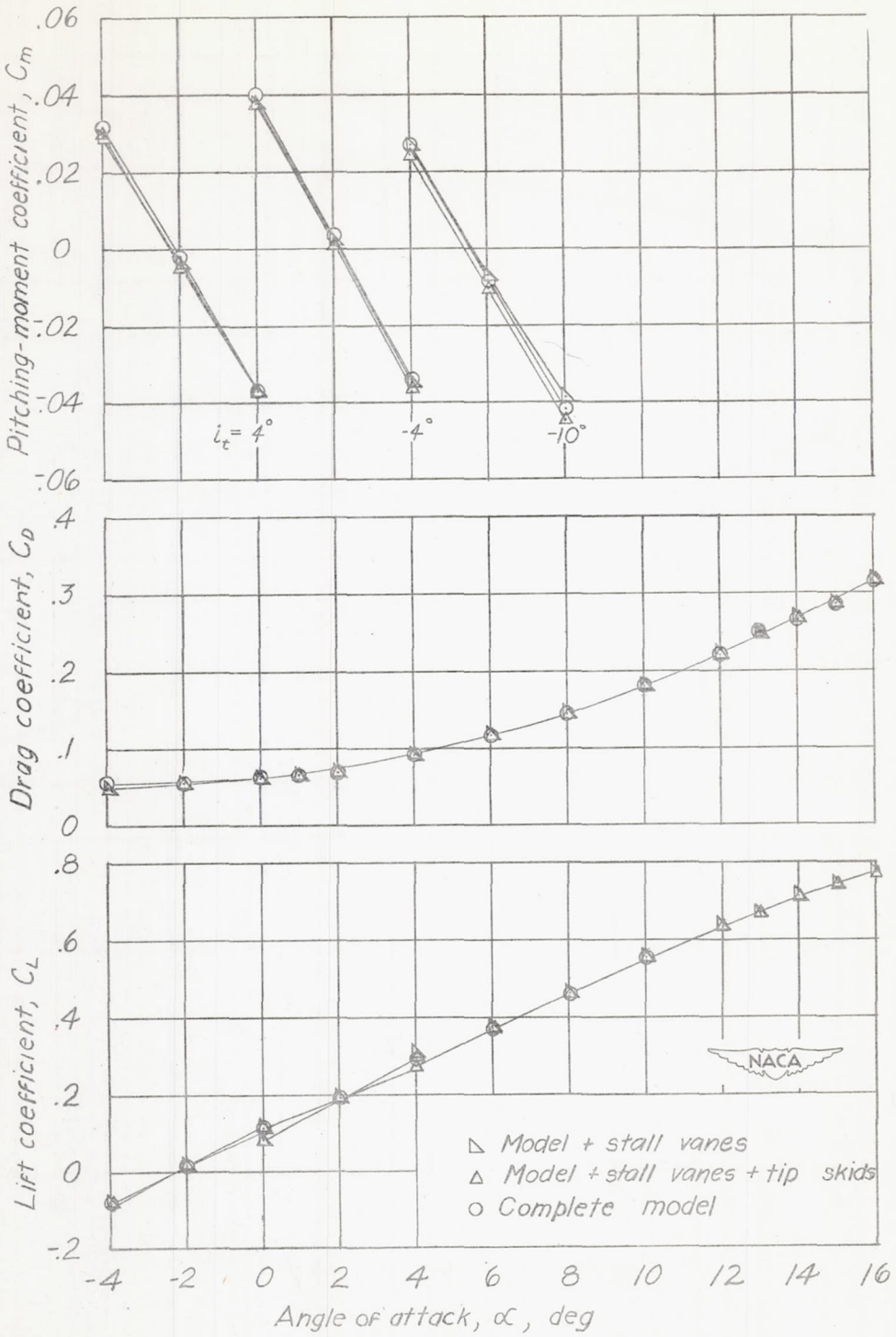

(a) Longitudinal characteristics.

Figure 25.- Effects of stall-control vanes and wing-tip skids upon the aerodynamic characteristics of the complete model. M = 1.59.

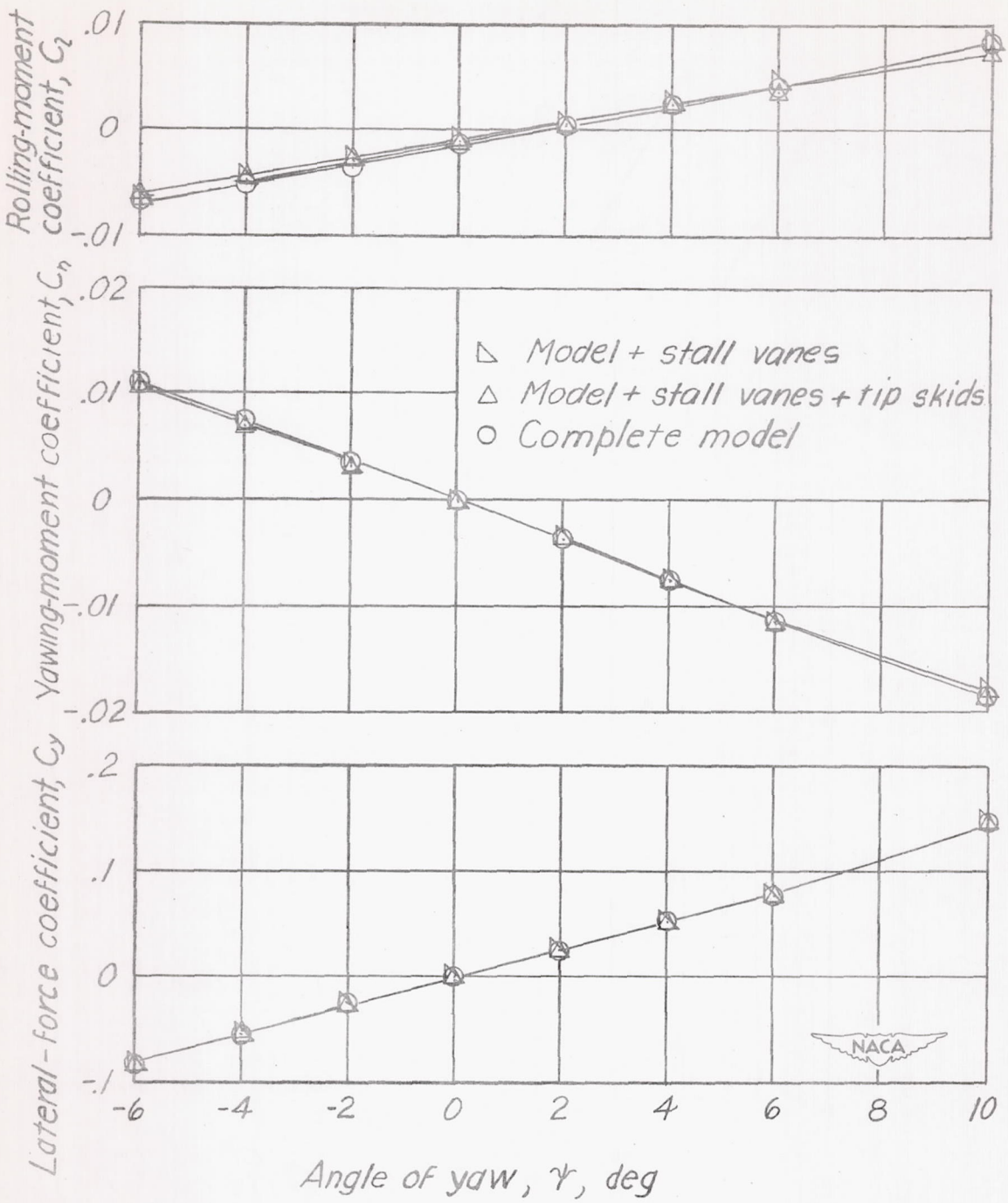

(b) Lateral characteristics.
$\alpha = 0$; $i_t = 0°$.

Figure 25.- Concluded.